

POLARIZATION OF ELECTRON AND PROTON BEAMS

J. Buon

Laboratoire de l'Accélérateur Linéaire, IN2P3-CNRS
et Université de Paris-Sud, France

J. P. Koutchouk

CERN, Geneva, Switzerland

Abstract

After defining the concept of polarization vector, its dynamics in static electro-magnetic fields is described in terms of the Thomas-BMT equation. The periodic orbital motion in circular machines is shown to excite spin resonances; they perturb the spin precession and cause depolarization. The acceleration of polarized protons illustrates the methods developed to avoid or weaken the depolarization. In electron rings, the consequence of synchrotron radiation is analysed in terms of spontaneous (Sokolov-Ternov) polarization and spin diffusion in presence of optics imperfections. It is shown how the spontaneous polarization can be used to determine with great accuracy the beam energy. Finally the local rotation of the spin in the direction of the velocity to allow colliding-beam experiments is discussed.

1. INTRODUCTION

1.1 Physics motivation

Spin is an important feature of nuclei and subnuclear particles, as well as their mass and electric charge. In general, the particle interactions depend to various degrees on their spin states. Experimental studies of these interactions with polarized beams and targets revealed important and new aspects of Nature. For instance, at SPEAR [1], the e^+e^- annihilation into multi-hadrons has been studied at 7.4 GeV center-of-mass energy. The angular distribution of the final state particles was found consistent with the quark-parton model; the data obtained with polarized beams confirmed that quarks are spin-1/2 particles. At Saturne II [2], experiments using polarized proton and deuteron beams on polarized proton targets have allowed an extensive study of the nucleon-nucleon scattering at intermediate energies.

Nowadays, the interest in polarized electron beams at high energies has come up again to test the Standard Model of the electro-weak interaction. In this model, the production of the Z vector boson with longitudinally polarized e^+e^- beams is left-right asymmetric. An accurate measurement of the asymmetry can give information on the mass range of the top quark and Higgs boson. Another example of the relevance of polarized beams is the study of the distribution of the angular momentum inside the nucleons.

A less direct but important contribution is to make possible an extremely accurate measurement of the beam energy and hence of the mass of the particles created in the e^+e^- annihilations. This is illustrated by the figures of Table 1 taken from [3] and by the present campaign of measurement of the mass and width of the Z particle at LEP.

Table 1
Improvement of the determination of particle masses
obtained from resonant depolarization of polarized e^+e^- beams

Particle	World average value (MeV)	Experimental results (MeV)	Year publication	Accuracy improvement
K^\pm	493.84 \pm 0.13	493.670 \pm 0.029	1979	5
K^0	497.67 \pm 0.13	497.661 \pm 0.033	1987	4
ω	782.40 \pm 0.20	781.780 \pm 0.10	1983	2
ϕ	1019.7 \pm 0.24	1019.52 \pm 0.13	1975	2.5
J/ψ	3097.1 \pm 0.90	3096.93 \pm 0.09	1981	10
ψ'	3685.3 \pm 1.20	3686.00 \pm 0.10	1981	10
Υ	9456.2 \pm 9.50	9460.59 \pm 0.12	1986	80
Υ'	10016.0 \pm 10.	10023.6 \pm 0.5	1984	20
Υ''	10347.0 \pm 10.	10355.3 \pm 0.5	1984	20

1.2 Historical summary

In the early sixties, knowledge of beam polarization and the associated technology allowed one to contemplate the acceleration of polarized particles: Froissart and Stora [4] calculated the depolarization on spin resonances for protons while Bargmann, Michel and Telegdi [5] reformulated the Thomas equation for the spin precession in arbitrary electromagnetic fields. Ternov, Lostukov and Korovina [6] discovered theoretically the spontaneous polarization of electrons in a magnetic field, which was analysed in detail by Sokolov and Ternov [7]. In 1970, radiative polarization was indeed observed and studied at ACO (Orsay) [8,9] and at VEPP-2 (Novosibirsk) [10,11] at about 0.5 GeV. Soon after, polarized protons were accelerated up to 12 GeV in the ZGS (Argonne) [12].

The last two decades have seen the development of techniques to accelerate polarized beams at higher and higher energies. Polarized protons have been successfully accelerated in several synchrotrons. At Saturne (Saclay) [13,14] beams of 2×10^{11} protons/burst, fully polarized, are routinely accelerated at energies up to 3 GeV. The maximum energy of 22 GeV [17] has been reached at the AGS (Brookhaven) [15]. Acceleration of polarized particles in the latest projects (RHIC, SSC) has been considered. Polarized electron beams

have also been accelerated at the Bonn 2.5 GeV synchrotron [16], at the high-energy linac of SLAC to 22 GeV [17] and recently up to 46 GeV at the Stanford Linear Collider (SLC) [18]. The most outstanding observation is the in-situ polarization build-up of electron beams circulating in large storage rings (HERA [19], Tristan [20]) up to the highest energy of 46 GeV at LEP [21], in spite of the potentially very strong depolarization phenomena.

1.3 Outline of the lecture

The first section introduces the concept of polarization for a spin-1/2 particle beam; the spin motion in static fields is discussed and the depolarizing effects explained by the coupling between the spin precession and the orbital motion in the accelerator. The enhancement of the depolarization by resonant mechanisms is studied and the different kinds of spin resonances arising in circular accelerators are given.

The second section deals more specifically with the acceleration of polarized protons in synchrotrons (see also previous reviews [22,23,24]). The depolarization due to resonance crossing during acceleration and the cures applied are discussed. One of the most promising techniques to overcome depolarization, the "Siberian snake", is presented as well as its first experimental tests.

In the last section, the specific case of relativistic electron beams in storage rings is considered (see also previous reviews [25,26,27]). The in-situ polarizing mechanism due to synchrotron radiation (the Sokolov-Ternov effect) is introduced. In the presence of optics imperfections the synchrotron radiation is also responsible for a harmful spin diffusion. This depolarizing mechanism, enhanced on spin resonances, is discussed as well as ways to improve polarization. The method to accurately calibrate an electron ring in energy, by crossing an RF resonance applied on purpose, is described. Finally, the spin rotators, which allow the rotation of the polarization vector from its natural vertical direction to the direction of the particle velocity, are presented as well as the requirements they must fulfill to avoid depolarization.

The polarized sources and the polarimeters are beyond the scope of this lecture. We avoided the SU(2) algebra, not essential and not familiar in accelerator physics, and formal proofs of the basic equations. We have preferred to limit ourselves to an analysis of the physical contents of the basic equations and of their consequences, illustrated by experimental results.

2. GENERAL SPIN DYNAMICS

2.1 Polarization of a spin-1/2 particle beam

2.1.1 Spin and magnetic moment

The spin of a particle is an internal degree of freedom which behaves like angular momentum. It is represented by the quantum vectorial operator $\hat{\mathbf{S}} = \{\hat{S}_x, \hat{S}_y, \hat{S}_z\}$. The class of spin $s = 1/2$ particles (electrons, muons, protons, neutrons, ..) corresponds to the eigenstates of $\hat{\mathbf{S}}^2$ with eigenvalue $s(s+1) = 3/4$. With respect to an arbitrary quantization axis Oz , a spin-1/2 particle can only be found in one of the two eigenstates of \hat{S}_z with the eigen values $S_z = +\hbar/2$ ("up" state) or $S_z = -\hbar/2$ ("down" state). \hbar is the Planck constant divided by 2π .

A magnetic moment $\hat{\mu}$ proportional to the spin $\hat{\mathbf{S}}$ is associated to a spinning charged particle:

$$\hat{\mu} = \frac{g}{2} \frac{e}{m_0} \hat{\mathbf{S}} = (1+a) \frac{e}{m_0} \hat{\mathbf{S}} \quad (1)$$

where e and m_0 are respectively the electric charge and the rest mass of the particle. The gyromagnetic ratio g is 2 for a point-like spin-1/2 particle in the Dirac theory. For real particles its deviation from 2 is expressed by the gyromagnetic anomaly [28] $a = (g - 2)/2$ (very often designated by G in the literature):

electron	muon	proton
$a = 1.5965 \times 10^{-3}$	1.16592×10^{-3}	1.79285

In a field of magnetic induction \mathbf{B} , the magnetic energy \hat{W} of a charged particle at rest is given by :

$$\hat{W} = -\hat{\mu} \cdot \mathbf{B} \quad (2)$$

2.1.2 Polarization of a single particle

A single spin-1/2 particle in a pure spin state along a given direction is fully polarized. Its polarization vector \mathbf{P} is the unit vector along that direction. In general, a particle is in a mixed state, i.e. it can be found in any of the pure spin states with a certain probability distribution. Its polarization vector is the distribution-weighted average of the polarization vectors of the pure spin states. The degree of polarization is the modulus of \mathbf{P} , in general smaller than one. A particle is unpolarized when $|\mathbf{P}| = P = 0$. It can be shown that two mixed states having the same polarization vector cannot be distinguished. A mixed state of an electron can thus be considered as the incoherent superposition of the “up” and “down” states along the direction of \mathbf{P} with the probabilities $1/2 (1 \pm P)$. In an ideally planar ring for instance, the ultimate degree of polarization is 92.36%, corresponding to probabilities of 96.18% and 3.82% respectively. In a gedanken experiment where the particle would be duplicated at infinity in the same mixed state, the degree of the polarization is the asymmetry of the populations N_+ and N_- of the “up” and “down” states:

$$P = \frac{N_+ - N_-}{N_+ + N_-} \quad (3)$$

It can be shown that the polarization vector is the quantum average of the spin operator $\hat{\mathbf{S}}$ expressed in units of $\hbar/2$ when the particle is in a pure state.

$$\mathbf{P} = \frac{2}{\hbar} \langle \psi | \hat{\mathbf{S}} | \psi \rangle = \mathbf{S} \quad (4)$$

In the semi-classical description of the spin dynamics, it is by convention named the spin vector noted \mathbf{S} .

The same property is also valid for a mixed case. It follows from (4) that the asymmetry of a spin-dependent quantity is proportional to \mathbf{P} . For instance, in an experiment only sensitive to the longitudinal spin component (parallel to the particle velocity), it would be proportional to the longitudinal component of \mathbf{P} .

According to the general rules of quantum mechanics (Ehrenfest theorem), the quantum average of $\hat{\mathbf{S}}$ behaves as a classical quantity. Its evolution can be described by a classical deterministic equation which accounts for the motion in a static electromagnetic field, including quantum spin flips between the eigenstates due to interaction with a radiative field.

2.1.3 Polarization of a beam of particles

The particles in a beam are distributed in oscillation amplitudes, defining the beam emittances. The same spreading occurs for the spin vectors. For instance, in a proton beam, particles with very small betatron amplitudes may be fully polarized along the vertical direction; particles with larger amplitudes suffer spin precessions in the quadrupole fields and become unpolarized with respect to the vertical direction. The polarization vector \mathbf{P} of the beam of particles is the statistical average of the individual spin vectors. Its length is the polarization degree of the beam. A beam is unpolarized ($P = 0$) if the spin vectors point to all directions isotropically. It is fully polarized ($P = \pm 1$) if all the particles are in the same pure spin state. For the same reason as above, the polarization vector of a beam is a classical quantity. The general approach to evaluate the beam polarization is to study the dynamics of the individual spin vectors and average over the six orbital coordinates of the particles to obtain the beam polarization.

This description of the beam polarization can be extended to the case of a deuteron beam. Deuterons are particles of spin 1 with three eigenstates $S_z = +\hbar, 0, -\hbar$ along any direction Oz . Their gyromagnetic anomaly [29] is $g = -0.142562$. The polarization vector \mathbf{P} is again the statistical and quantum average of the spin quantum operator $\hat{\mathbf{S}}$ and is mostly sufficient to determine the polarization state. The acceleration of polarized deuterons is similar to the acceleration of protons and even easier.

2.2 Spin precession in a static electromagnetic field

2.2.1 Non-relativistic particles

For non-relativistic non-radiating particles, the simplest way to establish the motion of the spin is to apply the fundamental law of classical mechanics: the rate of change of the angular momentum is equal to the torque exerted by the external field:

$$\frac{d\mathbf{S}}{dt} = \boldsymbol{\mu} \times \mathbf{B} \quad (5)$$

Expressing $\boldsymbol{\mu}$ in (5) in terms of \mathbf{S} according to (1) yields the Thomas equation:

$$\frac{d\mathbf{S}}{dt} = \Omega_L \times \mathbf{S} \quad (6)$$

This is the equation of a rotation (precession) of the spin vector \mathbf{S} around the direction defined by the rotation vector Ω_L , colinear to the magnetic field \mathbf{B} (Fig.1). The modulus of the rotation vector is the Larmor frequency.

$$\Omega_L = -\frac{g}{2} \frac{e}{m_0} \mathbf{B} \quad (7)$$

This precession is similar to the velocity rotation in a magnetic field:

$$\frac{d\mathbf{v}}{dt} = \Omega_c \times \mathbf{v} \quad (8)$$

with

$$\Omega_c = -\frac{e}{m_0} \mathbf{B} \quad (9)$$

For point-like spin-1/2 particles ($g = 2$) the spin precession frequency is equal to the cyclotron frequency. The relative deviation of the spin precession frequency with respect to the cyclotron frequency is just the gyromagnetic anomaly a :

$$\frac{\Omega_L - \Omega_c}{\Omega_c} = a \quad (10)$$

The measurement of this deviation is the principle of all the "g-2" experiments that aim to measure the gyromagnetic anomaly.

2.2.2 Relativistic particles

In an electromagnetic field a relativistic particle experiences an acceleration. To transform the electro-magnetic fields from the laboratory to the accelerated rest frame of the particles, a double Lorentz transform is required [30]. The spin precession retains the same law as (6), albeit with a different rotation vector. In this form, it takes its name from Bargman, Michel and Telegdi [5] (abbr. BMT equation) :

$$\frac{d\mathbf{S}}{dt} = \Omega_{BMT} \times \mathbf{S} \quad (11)$$

with :

$$\Omega_{BMT} = -\frac{e}{m_0\gamma} \left[(1 + a\gamma)\mathbf{B}_\perp + (1 + a)\mathbf{B}_\parallel - \left(a + \frac{1}{\gamma + 1} \right) \gamma \boldsymbol{\beta} \times \frac{\mathbf{E}}{c} \right] \quad (12)$$

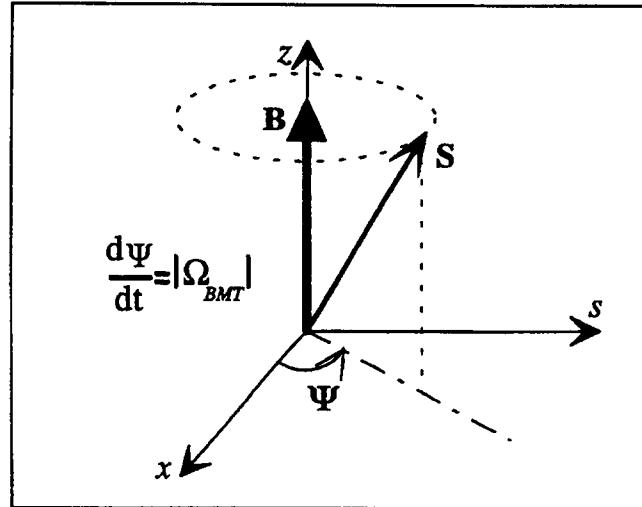


Fig 1: Precession of the spin vector \mathbf{S} about the magnetic field \mathbf{B} .

where \mathbf{B}_\perp (\mathbf{B}_\parallel) is the transverse (longitudinal) component of the induction \mathbf{B} relative to the particle velocity ; γ is the relativistic Lorentz factor and β is the velocity in units of the light velocity c . In that equation the fields \mathbf{E} and \mathbf{B} and the time t are expressed in the laboratory frame (all quantities in MKS units). On the other hand, the spin vector \mathbf{S} is expressed in the instantaneous rest frame of the particle and the BMT equation includes the Thomas precession [31,32] that occurs in that frame.

The spin precession has the following general properties :

- The rotation in an electric field \mathbf{E} or a magnetic field $\mathbf{B} = \mathbf{E}/c$ is of the same order of magnitude: an electric field of 3×10^8 V/m has a rotating strength comparable to that of a 1 Tesla magnetic field. Applied electric fields in accelerators are in general smaller and their effect on the spin negligible. However, it results from the Lorenz transformations that the electric and magnetic forces between two charged and ultra-relativistic particles have asymptotically the same modulus. They cancel out when the velocities are parallel, e.g. in the same beam, but add to each other when the velocities are anti-parallel, e.g. when the beams are colliding. For the spin precession, the same property results from the BMT equation.
- The spin rotating strength of a field \mathbf{B}_\parallel parallel to the velocity is inversely proportional to the particle momentum \mathbf{p} , as the velocity rotating strength of a transverse field \mathbf{B} is. The parallel-field integral needed to rotate the spin by one radian is :

$$\int \mathbf{B}_\parallel ds \text{ (Tm/rad)} = -\frac{1}{1+a} \frac{\mathbf{p}}{e} \approx -\frac{10.479}{\pi(1+a)} \mathbf{p} \quad (13)$$

At 1 GeV/c, a parallel-field integral of 10.479 Tm is needed to rotate the spin by 180° for a particle with vanishing gyromagnetic anomaly.

- The difference in frequency of spin and velocity precessions about a transverse magnetic field \mathbf{B}_\perp

$$\Omega_a = \Omega_{BMT} - \Omega_c = \gamma a \left[\frac{e}{m_0 \gamma} \mathbf{B}_\perp \right] \quad (14)$$

is exactly independent of the particle energy, and is γa times larger than the relativistic cyclotron frequency $\Omega_c = e\mathbf{B}_\perp / m_0\gamma$.

$$\Omega_a = \gamma a = \Omega_c \quad (15)$$

The vector Ω_a is the spin rotation vector with respect to a frame attached to the particle trajectory (the so-called orbit frame); the latter rotates at the cyclotron frequency Ω_c following the velocity β .

- The transverse-field integral required to rotate the spin by one radian with respect to the orbit frame is slightly dependent on the energy through the relativistic velocity

$$\int \mathbf{B}_\perp ds (\text{Tm/rad}) \approx -\frac{5.484}{\pi} \beta \quad \text{for a proton,} \quad (16)$$

$$\int \mathbf{B}_\perp ds (\text{Tm/rad}) \approx -\frac{4.618}{\pi} \beta \quad \text{for an electron} \quad (17)$$

In a given transverse field, the spins of protons and electrons precess by comparable amounts: the larger mass of the proton is compensated by its larger gyromagnetic anomaly.

- At high energies, when $\gamma a \gg 1$, the spin rotation by transverse fields becomes nearly energy-independent while the spin rotation by longitudinal fields becomes less and less effective. Transverse fields are preferred for spin manipulations at high energies. Moreover, the spin rotation requires much less bending field than the trajectory does and the spin vector precesses much faster than the particle velocity. For example, the spin precesses 103.5 times per machine revolution at the 45.6 GeV in LEP (Z production energy), i.e. in about 0.1 ms. The time scale of this process is in great contrast with that of the spontaneous polarization (minutes to hours), as we shall see later, and with the time it takes to emit a photon (typically 10^{-10} s). This makes it possible to study separately the polarizing and depolarizing phenomena.

2.3 Spin precession in a circular particle accelerator

2.3.1 Ideal accelerator

As we have seen above, the spin motion in a constant magnetic field is a simple precession. Calculating the spin motion in an ideal accelerator or storage ring is a straightforward extension but allows one to introduce the formalism necessary to treat the general case. All the elements (dipoles, quadrupoles, sextupoles) of the ideal ring are supposed to lie in the same plane, e.g. horizontal. At any energy, the closed orbit lies in the same horizontal plane. A vertical spin of a particle circulating on the closed orbit will stay vertical, parallel to the guide field. This constant spin direction is called the spin closed solution \mathbf{n}_0 .

Any other spin direction precesses about the spin closed solution \mathbf{n}_0 , vertical in this case. The number ν of spin precessions per orbit revolution is found by replacing Ω_c by 2π in (15):

$$\nu = a\gamma \quad (18)$$

i.e. numerically:

	electrons	protons	deuterons
$\nu =$	$\frac{E(\text{GeV})}{0.44065}$	$\frac{E(\text{GeV})}{0.52335}$	$\frac{E(\text{GeV})}{13.1565}$

as a function of the total relativistic energy E . Unlike the betatron tunes, the spin tune increases linearly with the energy.

In fact, the magnetic fields are distributed in a piece-wise way along the orbit. The spin precesses in the bending magnets and remains constant in straight-sections as long as the trajectory passes the quadrupoles on-axis. If the spin precession is Fourier-analysed with respect to the machine azimuth, the spectrum of the spin precession is no longer a single line; it shows instead satellites at $\pm k$, $k \in N$, which reflect the distribution and symmetry of the bending magnets.

Particles experiencing horizontal betatron oscillations and synchrotron oscillations are confined to the horizontal plane. The vertical direction is again the spin closed solution \mathbf{n}_0 . The spin precession frequency about \mathbf{n}_0 is still $\nu = a\gamma$ on average. The spectral analysis shows however satellites at $\pm kQ_x$ and $\pm kQ_s$, $k \in N$ where Q_x and Q_s are the betatron and synchrotron tunes. These satellites are due to the extra spin rotations caused by the non-vanishing amplitudes of the beam oscillations in the quadrupoles and sextupoles. For all these horizontal trajectories, the vertical spin component S_z is conserved; there is thus a strong incentive to have circulating beams with a vertical polarization.

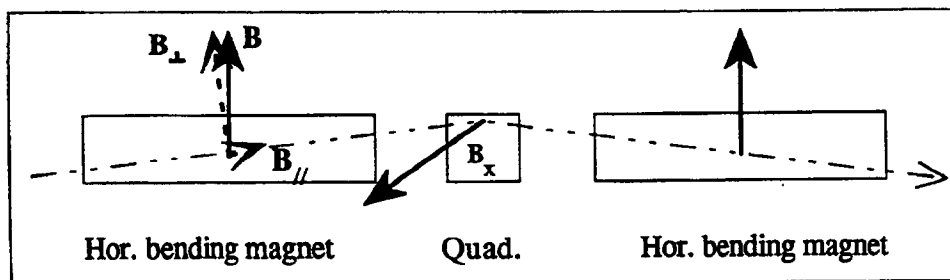


Fig. 2: Fields along a trajectory oscillating in the vertical plane and passing through horizontally bending magnets and quadrupoles.

Even in an ideal accelerator, beams of non-radiating particles are subject to vertical betatron oscillations due to the finite vertical emittance. Along this vertical betatron oscillation, the field \mathbf{B}_x in the quadrupoles is horizontal and proportional to the vertical displacement (see Fig. 2). A small parallel field $\mathbf{B}_{//}$ is also experienced in the horizontally bending magnets

where the trajectory has a vertical slope. The spin is thus bent away from the vertical direction, in a trajectory dependent way. This phenomenon is called *spin-orbit coupling*. At 46 GeV in LEP for instance, the spin precession in an arc quadrupole is $\Delta\psi = a\gamma Kl \cdot \Delta y \approx 2.5$ mrad/mm with Kl integrated gradient and Δy vertical beam displacement in the quadrupole. Even in an ideal accelerator, the spin-orbit coupling may give rise to depolarization. It can be minimized by reducing the vertical beam emittance or by special optics provisions which, by counteracting the spin-orbit coupling, allow to recover the spin transparency of the ideal accelerator. (See sections 4.3, 4.4.)

2.3.2 General case

Although, in general, particle accelerators are designed to lie in a plane, the unavoidable imperfections of alignment and of the magnetic fields break the symmetry about the horizontal plane. In many cases, vertical deflections or solenoidal fields are even introduced on purpose to combine or separate colliding beams, provide means to analyse the products of beam-beam interactions or rotate the spin. On the non-planar closed orbit, the spin is subject to successive rotations in the magnetic elements as the particle makes one revolution starting at azimuth s . Unlike the case of the ideal accelerator, these rotations occur about different axes. The one-turn mapping of the spin is the product of the local spin rotations and is a rotation itself $\mathbf{T}(s)$. The real eigenvector of the rotation matrix is the only vector which, transported by the Thomas-BMT equation once around the ring, reproduces itself:

$$\mathbf{n}_0(s) = \mathbf{T}(s)\mathbf{n}_0(s) \quad (19)$$

It is easy to prove that the one-turn rotation axes $\mathbf{n}_0(s)$ along the machine can all be deduced from each other by virtue of the BMT equation. Let us consider two azimuths s_0 and s_1 , where the one-turn mappings are \mathbf{T}_0 and \mathbf{T}_1 with eigenvectors \mathbf{n}_{00} and \mathbf{n}_{01} (Fig. 3).

Let \mathbf{R}_{01} be the spin transport matrix from s_0 to s_1 . The principle is to express the transport \mathbf{T}_0 as a function of \mathbf{T}_1 in the equation of \mathbf{n}_{00} :

$$\mathbf{n}_{00} = \mathbf{T}_0\mathbf{n}_{00} = \mathbf{R}_{01}^{-1}\mathbf{T}_1\mathbf{R}_{01}\mathbf{n}_{00} \quad (20)$$

Hence

$$\mathbf{R}_{01}\mathbf{n}_{00} = \mathbf{T}_1\mathbf{R}_{01}\mathbf{n}_{00} \quad (21)$$

$\mathbf{R}_{01}\mathbf{n}_{00}$ is by definition the real eigenvector \mathbf{n}_{01} of \mathbf{T}_1 , i.e. \mathbf{n}_{01} is obtained from \mathbf{n}_{00} by the spin transport from s_0 to s_1 . $\mathbf{n}_0(s)$ is thus the spin closed solution. Because rotations conserve angles, any other spin direction will appear to precess about it, much like a betatron oscillation around the closed orbit. As we already saw, the spin closed solution is vertical in an ideal ring lying in a horizontal plane. Usually horizontal bending fields are small and the spin closed solution is nearly vertical. The one-turn spin precession $2\pi\nu$ is given by the phase angle of the two imaginary eigenvalues of the one-turn matrix $\mathbf{T}(s)$. It is independent of the azimuth s since \mathbf{T}_0 and \mathbf{T}_1 are similar matrices owing to (20). Hence

$$2\pi\nu = \cos^{-1} \left(\frac{\text{Trace}(\mathbf{T}(s)) - 1}{2} \right), \quad \forall s \quad (22)$$

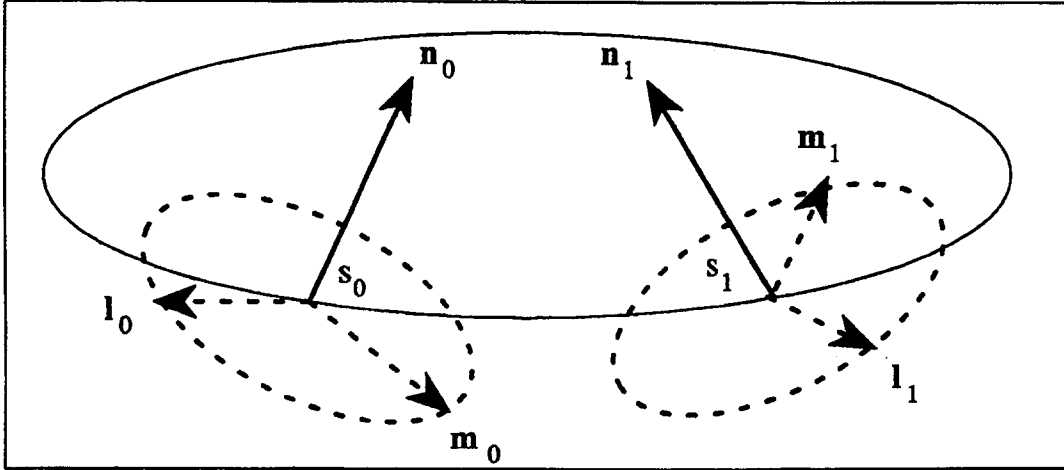


Fig. 3: Transport of the orthogonal spin frame $(\mathbf{l}_0, \mathbf{m}_0, \mathbf{n}_0)$ from s_0 to s_1 .

In an ideal ring, the spin tune was shown to be simply related to the energy (18). In a real ring with small vertical bends, this is not true any more. In general, the deviation is very small and can be ignored. It may however set a limit to the accuracy of the calibration by resonant depolarization, as will be shown later. In special cases, the spin precession is perturbed on purpose by large rotations which shift the spin tune. The extreme is the "Siberian snake"[33,34] which enforces half-integer spin values, whatever the particle energy. This special insertion will be analysed later (see section 3.3).

So far we considered the particle motion on the closed orbit. Particles oscillate about it with three degrees of freedom. The oscillation amplitudes being generally small (but not always), the resultant spin precessions may be considered as a perturbation of the spin motion on the closed orbit. It is thus convenient to consider the spin motion in a frame which eliminates the spin motion on the closed orbit. Such an orthonormal frame $(\mathbf{l}_0, \mathbf{m}_0, \mathbf{n}_0)$ is obtained by associating to the spin closed solution $\mathbf{n}_0(s)$ two orthogonal spin solutions $\mathbf{l}_0(s)$ and $\mathbf{m}_0(s)$ precessing around $\mathbf{n}_0(s)$ by $2\pi\nu$ in one revolution. At this point, it should be noted that the calculation of the electron depolarization requires a more general definition of \mathbf{n} on any non-periodic trajectory which coincides with \mathbf{n}_0 on the closed orbit. To simplify the notation, $(\mathbf{l}_0, \mathbf{m}_0, \mathbf{n}_0)$ will be noted $(\mathbf{l}, \mathbf{m}, \mathbf{n})$ unless the more general definition is required.

Along the perturbed orbital trajectories, the spin-orbit coupling is responsible for beam depolarization. The spread of energies and trajectories among the particles in a beam leads to a spread in the spin precession. Assuming that all the individual spins would initially point to the same direction (full polarization), after some time they will spread in different directions. The modulus of the beam polarization vector, i.e. the degree of polarization, decreases. As we shall

see later, the depolarization due to the spin-orbit coupling shows resonant properties. Minimizing the depolarization requires the minimization of the spin-orbit coupling and a selective compensation of the most important spin resonances. The conditions to fulfill are referred as the "spin transparency conditions [35]" obtained by "spin matching". (See sections 4.3, 4.4.)

Returning to the spin motion on the closed orbit, one might think that, because the spin and the velocity follow the same dynamics as given by equations (8) and (11), the spin should be restored when the orbit angle is restored. This is not so: unlike the orbit, the spin experiences large rotations in the orbit frame due to the dipole field. For example, the spin precesses by 1.2 rad in each LEP 1/2 cell at 46 GeV. Because of the non-commutativity of finite rotations, the spin is not restored if the orbit is. This is illustrated in Fig. 4: in Fig. 4a, the vertical orbit is locally perturbed between points A and B by exciting a π -bump; the tip of the spin vector, seen from above, is shown not to be restored on Fig. 4b.

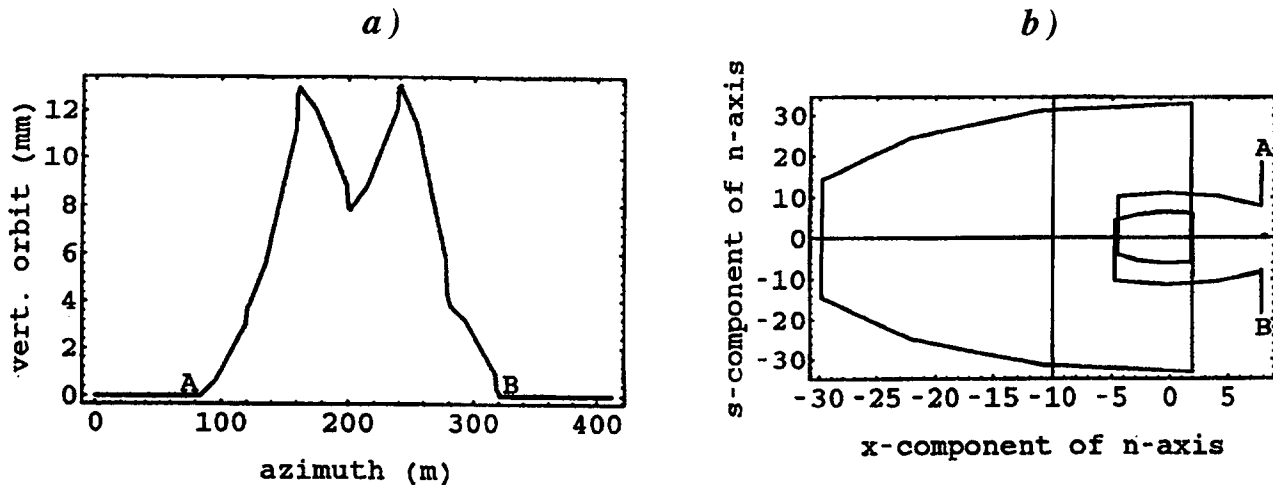


Fig. 4: Rotations of the orbit (closed bump) in *a*) and of the spin in *b*).

This property allows one to manipulate the spin direction by modifying locally the closed orbit. At high energy where the spin is much easier to rotate than the velocity, these bumps can be made relatively small and can be optically matched to the rest of the ring. Spin rotators and "Siberian snakes" become conceivable insertions.

2.3.3 Spin-dependent orbit perturbation

So far, we considered the consequences of the torque exerted by the magnetic force on the magnetic moment of the particle. This is not the only interaction in addition to the usual Lorentz force. If the gradient of the magnetic field does not vanish, the particle momentum receives a kick $\int \mathbf{F} ds$ due to the interaction of the magnetic moment with the field gradient:

$$\mathbf{F} = \boldsymbol{\mu} \cdot \nabla \mathbf{B} \quad (23)$$

This is the reverse of the spin-orbit coupling. Different spin states lead to slightly different trajectories as observed in experiments of the Stern-Gerlach type. However, the reverse coupling is very weak at high energies: the spin-dependent kick produced by a quadrupole in

LEP is the same as the kick produced by the same quadrupole displaced by $4.5 \cdot 10^{-13}$ mm! The magnetic energy of a spin state is indeed of the order of $ae \hbar / 2m \approx 10^{-13}$ MeV/Tesla, much smaller than the kinetic energy. Another tiny effect arises from the slight dependence of the synchrotron radiation emitted by electrons on their spin state. The beam emittance should be insignificantly modified.

2.4 Spin resonances

2.4.1 Resonant perturbation of the spin motion

When the spin-orbit coupling is not so strong as to depolarize the beam completely, the dependence of the polarization level on the spin tune is observed to be remarkable (e.g. Fig. 23). The polarization vanishes or is minimum at several distinct places where the spin tune is found to fulfill the relationship:

$$\nu = k + k_x Q_x + k_z Q_z + k_s Q_s \quad (24)$$

where Q_x , Q_z and Q_s are respectively the horizontal, vertical betatron tunes and the synchrotron tune, and the k 's are signed integers. This is a signature of coupling resonances between the spin degree of freedom and the three orbit degrees of freedom. They are called spin resonances.

Whenever the trajectory is not ideal, i.e. does not go through the magnets on their magnetic axis, a perturbing magnetic field $\mathbf{b}(s)$ is experienced. Its component \mathbf{b}_\perp , perpendicular to the main precession axis, bends the spin vector \mathbf{S} of the oscillating particle away from it. This field perturbation may be static, if due to an imperfect closed orbit, or oscillating with the betatron and synchrotron motions. The perturbation of the spin motion is superimposed on the nominal precession in the guide field. Depending on the phase relationship between spin precession and perturbation, a resonant spiraling motion can occur, generally causing a fast depolarization (Fig.5).

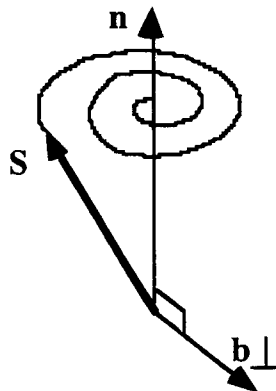


Fig. 5: On a spin resonance the spin vector \mathbf{S} , bent away from the spin closed solution \mathbf{n} by a perpendicular perturbing magnetic field \mathbf{b}_\perp , spirals out about \mathbf{n} .

The resonance phenomenon is best understood when using a simple model of a single spin resonance. For that purpose, we specify a perturbing field $\mathbf{b}_\perp(s)$, orthogonal to the unperturbed spin closed solution $\mathbf{n}(s)$, which is assumed to rotate about $\mathbf{n}(s)$ at the frequency ν_r . If ν_r significantly differs from the spin precession frequency (assumed to be uniform), the phase difference between the motions of a spin \mathbf{S} and of $\mathbf{b}_\perp(s)$ linearly increases with time. The successive kicks on the spin vector \mathbf{S} point to different directions and average to zero in a finite time. In spite of the perturbing field there is no significant depolarization. On the contrary, when ν_r and ν coincide, the phase difference between the motions of \mathbf{S} and of $\mathbf{b}_\perp(s)$ is stationary and the kicks add up constructively (Fig. 6). In addition to its precession about \mathbf{n} , the spin vector \mathbf{S} is then subject to an orthogonal rotation about $\mathbf{b}_\perp(s)$ at the frequency

$$\varepsilon = (1 + \gamma a) \frac{b_\perp}{B_0} \quad (25)$$

in units of the revolution frequency Ω_c , where B_0 is the field of the nominal bending magnets. The combination of these two rotations gives the spiraling motion of the spin vector.

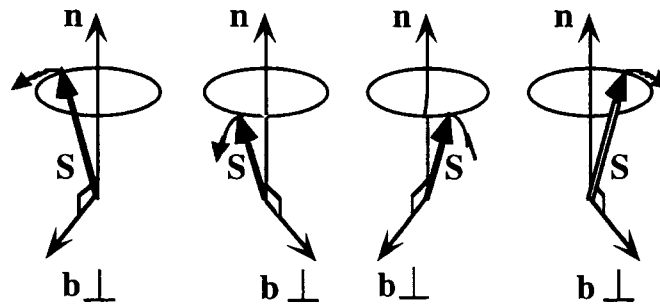


Fig. 6: The directions of a spin vector \mathbf{S} and of the perturbing field \mathbf{b}_\perp at different times on a spin resonance. The dashed arrows show the directions of the kicks given to \mathbf{S} , all of them bending it away from \mathbf{n} .

A better way to study spin resonances is to look at the spin motion in the $(\mathbf{l}, \mathbf{m}, \mathbf{n})$ frame which rotates about \mathbf{n} at the frequency ν (section 2.3.2). In this frame, the perturbing field \mathbf{b}_\perp rotates at the frequency $\nu_r - \nu$. On top of the resonance ($\nu_r = \nu$), it becomes stationary and the successive kicks given to a spin \mathbf{S} add up constructively and lead to a continuous spin rotation about \mathbf{b}_\perp . This rotation periodically exchanges the two spin states "up" and "down". Such a spin resonance is exactly what happens in a Nuclear Magnetic Resonance experiment. The polarized beam is the analogue of a substance with spin-aligned nuclei. The field of the normal bending magnets is the analogue of the DC magnetic field applied to the magnetized substance. The perturbing field \mathbf{b}_\perp plays the role of the applied RF field that resonates with the spin precession in a NMR experiment.

The frequency ε in (25) measures the speed at which the spin vector is bent away from the direction of \mathbf{n} . It is the strength of the resonance. It also measures the width of the resonance, as the tilt of \mathbf{S} is negligible when the frequency difference $\nu_r - \nu$ becomes larger than ε . In practical cases the perturbing fields can be expanded in sums of rotating components. Because the perturbing fields are caused by the trajectory displacements due to the deviations of the periodic orbit and to the betatron and synchrotron oscillations, the field

components rotate at frequencies which are linear combinations of the revolution, betatron and synchrotron frequencies. Likewise, the spin precession may be expanded in rotating components. A spin resonance occurs whenever a spin and field component rotate at the same frequency, as expressed by (24). The strength of the corresponding spin resonance is obtained by extracting from the perturbing field \mathbf{b}_\perp the component rotating at the resonant frequency ν_r . It is convenient to represent the rotation vector about \mathbf{b}_\perp in the (\mathbf{l}, \mathbf{m}) plane perpendicular to \mathbf{n} by a complex number ω :

$$\omega = (1 + \gamma a) \frac{(\mathbf{m} + i\mathbf{l}) \cdot \mathbf{b}}{B_0} \quad (26)$$

following (25). The ν_r rotating component is given by the corresponding Fourier component of ω :

$$\omega_r = \frac{1 + \gamma a}{2\pi B_0 \rho} \oint (\mathbf{m} + i\mathbf{l}) \cdot \mathbf{b} e^{2i\pi(\nu - \nu_r)s/R} ds \quad (27)$$

where the integration extends over one turn (the $e^{2i\pi\nu}$ phase factor compensates the phase advance of $\mathbf{m} + i\mathbf{l}$). The strength ε is the modulus of the Fourier component ω_r .

Depolarization occurs on a spin resonance when the perturbing field \mathbf{b}_\perp is different for each particle in the beam. The phase of \mathbf{b}_\perp may vary because the phases of the betatron and synchrotron oscillations are randomly distributed in the beam or because particles with different energies must cross the resonance condition at a different time. The amplitude of \mathbf{b}_\perp varies with the oscillation amplitudes. The individual spin directions become scattered in space, leading to a decrease of the beam polarization. The depolarization increases with the resonance strength ε , which itself increases with energy (25). To illustrate the sensitivity of the high energy machines, we show on Fig. 7 the calculated depolarization in an ideal LEP at 45 GeV, due to the horizontal component of the earth magnetic field ($0.2 \cdot 10^{-4}$ Tesla) which only perturbs the beam in the straight-sections. The spin resonances are so large as to require compensation.

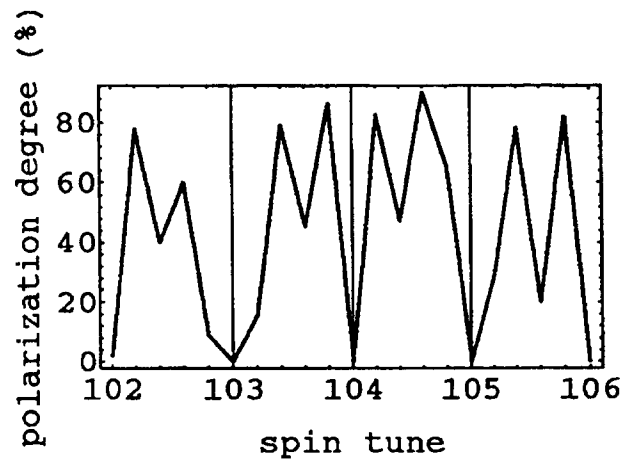


Fig. 7: Calculated depolarization by the uncorrected earth magnetic field in an otherwise ideal LEP.

At high energy, near-by resonances may overlap leading to a more complex polarization behaviour.

2.4.2 Classification of spin resonances

The condition for spin resonances (24) defines a dense web and one might think that one cannot avoid depolarizing resonances. However, calculations as well as measurements show that there is a hierarchy of spin resonances. Depending on the type of spin-orbit coupling, the beam energy or peculiarities of the accelerator, their depolarizing effect can be vastly different. The aim of a classification is to group resonances sharing common properties. The classification follows from the perturbing fields, symmetry or dynamics:

- the dipole fields drive the *integer* resonances $\nu = k$,
- the quadrupole fields drive the *linear* resonances $\nu = k + k_x Q_x + k_z Q_z + k_s Q_s$, with $|k_x| + |k_z| + |k_s| = 1$,
- the multipole fields drive the *non-linear* resonances where $|k_x| + |k_z| > 1$,
- the modulation of the field components by a finite-amplitude synchrotron motion drives *higher-order* synchrotron and synchro-betatron spin resonances with $|k_x| + |k_z| + |k_s| > 1$, $k_s \neq 0$.

The solenoidal fields drive both integer and linear resonances. Each type of spin resonance is repeated when the integer k is increased by one unit, i. e. every 523 MeV for protons and every 440 MeV for electrons. The various families of resonances are analysed in the following sections.

2.4.3 Integer spin resonances

The resonance condition of the integer (also named imperfection) resonances is

$$\nu = k \quad (28)$$

They are mainly produced by vertical closed orbit distortions when the spin closed solution \mathbf{n} is not radial and possibly by horizontal closed orbit distortions when \mathbf{n} is not vertical. These orbit distortions are caused by field errors and tilts of the bending magnets and by misalignment of quadrupoles and sextupoles. Systematic imperfections excite more selectively the resonances $\nu = kP$, where P is the machine superperiod. However, the dominant modulation of the resonance strength is related to the spectrum of the closed orbit. Random imperfections unexpectedly drive systematic integer spin resonances: the orbit spectrum is peaked at the betatron tune $Q_{x/z}$ unless the closed orbit is very carefully corrected. It is then possible to show that the resonances

$$\nu = \text{int}(Q_{x/z}) + k \cdot P_B \quad (29)$$

with P_B superperiod of the *bending* [36] are selectively excited and should be avoided.

On top of the resonance the perturbing dipole field perpendicular to the unperturbed \mathbf{n} is exactly stationary in the $(\mathbf{l}, \mathbf{m}, \mathbf{n})$ frame. A spin aligned along the perturbing field is also stationary. It is a particular solution of the perturbed spin motion, periodic in the laboratory frame. As it lies in the plane perpendicular to the unperturbed \mathbf{n} , the beam polarization will be periodically exchanged between the up and down states. Because a dipole field acts in the same way on all spins, there should be no depolarization. However side-effects may prevent the conservation of the length of the polarization vector. Due to the beam energy spread, all the particles in a beam do not cross an integer resonance at the same time during energy ramping; this causes a spread in precession phase and some depolarization. More important is the interplay between integer and linear resonances. The integer resonance is a resonant tilt of the \mathbf{n} -axis. This tilt in turn excites near-by linear resonances and causes them to overlap the integer resonances. In the high-energy electron machines, this mechanism causes strong depolarization. This is the reason why the compensation of the integer spin resonances is essential.

2.4.4 Linear spin resonances

These occur when only one of the k_x , k_z and k_s in (24) does not vanish and equals ± 1 . They are mainly produced by transverse quadrupole fields :

$$\mathbf{b} = \mathbf{x} \frac{\partial B_x}{\partial z} z + \mathbf{z} \frac{\partial B_z}{\partial x} x \quad (30)$$

where x and z are the trajectory displacements along the radial \mathbf{x} and vertical \mathbf{z} unit vector respectively. One distinguishes three types of linear spin resonances, corresponding to the coupling of the spin precession with each of the three degrees of freedom of the orbital motion.

1. *The vertical betatron resonances* (also named intrinsic resonances)

$$\nu = k \pm Q_z \quad (31)$$

are driven by vertical betatron oscillations

$$z = a_z \sqrt{\beta_z} \cos \phi_z \quad (32)$$

whenever the spin closed solution \mathbf{n} is not pointing to the radial direction \mathbf{x} . That is the general case as \mathbf{n} is nearly vertical in horizontal rings. One recognizes that the Fourier spectrum of \mathbf{b}_\perp is made of lines : $(k_o \pm Q_z) \Omega_c$, leading to the formula (31). Moreover, the integer k is a multiple of the ring superperiodicity. However, in real rings, small defects generally break the superperiodicity and weaker spin resonances appear at integer values k not multiples of the superperiodicity.

2. The horizontal betatron resonances

$$v = k \pm Q_x \quad (33)$$

are driven by horizontal betatron oscillations

$$x = a_x \sqrt{\beta_x} \cos \phi_x \quad (34)$$

whenever the spin closed solution is not exactly vertical. In general, this is due to small imperfections of the ring. It also occurs in a ring equipped with spin rotators which bends \mathbf{n} along the longitudinal direction in some sections of the ring. A horizontal betatron spin resonance can also result from an x - z coupling

$$z = \varepsilon \cos (Q_x \theta + \phi_x) \quad (35)$$

when \mathbf{n} is not radial.

3. The synchrotron resonances

$$v = k \pm Q_s \quad (36)$$

are driven by horizontal and vertical synchrotron oscillations :

$$\begin{aligned} x &= D_x \frac{\delta P}{P_o} \cos (Q_s \theta + \phi_s) \\ z &= D_z \frac{\delta P}{P_o} \cos (Q_s \theta + \phi_s) \end{aligned} \quad (37)$$

They are also due to imperfections as the horizontal oscillations only contribute when \mathbf{n} is not exactly vertical and the vertical oscillations only when the vertical dispersion D_z does not vanish. Because the synchrotron tune Q_s is often small, these resonances are referred to as synchrotron satellites. When the Q_s is very small ($Q_s \ll 1$), one usually does not disentangle the integer resonance from its satellites.

The strength of *linear* resonances can be expressed following (27) in an explicit way which is useful for resonance compensation. The strength of the *integer* resonance is hidden behind the calculation of the perturbed $(\mathbf{l}, \mathbf{m}, \mathbf{n})$ frame which can only be performed

numerically. Assuming this frame calculated, the strengths ε of the three types of *linear* spin resonances are respectively given by :

$$\begin{aligned}\varepsilon_{\pm z} &= a_z (1 + \gamma a) \left| \oint (\mathbf{m} + i\mathbf{l}) \cdot \mathbf{x} K \sqrt{\beta_z} e^{2i\pi(\nu \pm Q_z)s/R \pm i\phi_z} ds \right| \\ \varepsilon_{\pm x} &= a_x (1 + \gamma a) \left| \oint (\mathbf{m} + i\mathbf{l}) \cdot \mathbf{z} K \sqrt{\beta_x} e^{2i\pi(\nu \pm Q_x)s/R \pm i\phi_x} ds \right| \\ \varepsilon_{\pm s} &= \frac{\delta P}{P_0} (1 + \gamma a) \left| \oint (\mathbf{m} + i\mathbf{l}) \cdot K(D_x \mathbf{z} + D_z \mathbf{x}) e^{2i\pi(\nu \pm Q_s)s/R \pm i\phi_s} ds \right|\end{aligned}\quad (38)$$

K is the normalized gradient of the quadrupoles. The three integrals, named *spin-orbit coupling integrals*, express the amplitude of the spin-orbit coupling for each linear resonance. The strength is also proportional to the respective amplitude of oscillation a_x, a_z and $\delta P / P_0$ and to the energy. For a distribution of particles, it must be averaged over the amplitude distribution, and also over the relative phases of oscillations ϕ_x, ϕ_z, ϕ_s . It is worth noting the absence of parametric resonances $k + 1/2$. Therefore, the best energy to maintain a high degree of polarization in a storage ring normally corresponds to a half-integer spin tune, that is midway between linear spin resonances. It is also advantageous that the nearest integers should not be multiples of the ring periodicities.

2.4.5 Non-linear spin resonances

Non-linear spin resonances are produced by higher-order multipole fields :

$$\mathbf{b} \propto x^p z^q, \quad p + q > 1 \quad (39)$$

The frequency analysis of \mathbf{b} leads to a resonant condition of the type :

$$\nu = k_o + k_x Q_x + k_z Q_z \quad (40)$$

with $|k_x| \leq p$ and $|k_z| \leq q$. For instance a sextupole field will drive non-linear resonances with $|k_x| + |k_z| = 2$. The beam-beam interaction in storage rings will also drive series of non-linear resonances.

2.4.6 Higher-order spin resonances

Another family of resonances plays an important role at high energy when the amplitude of the synchrotron oscillations becomes large. In contrast with the preceding resonances, the perturbation of the spin motion is due to the component of the perturbing field along \mathbf{n} , mainly produced by the horizontal synchrotron oscillations. It causes a perturbation of the spin precession frequency ω that can be analysed as a modulation of the spin tune at the frequency of the synchrotron oscillations Q_s .

$$\nu_0 - k_s Q_s \quad |k_s| \geq 1 \quad (41)$$

Several synchrotron satellites appear on each side of any depolarization resonance ($\nu = \nu_r$) of the preceding types:

$$\nu = \nu_r + k_s Q_s \quad |k_s| \geq 1 \quad (42)$$

This modulation is proportional to the energy spread and increases rapidly with the particle energy.

3. ACCELERATION OF POLARIZED PROTONS IN SYNCHROTRONS

3.1 Experimental observations and results

Polarized protons have been successfully accelerated at high energies (larger than one GeV) in several synchrotrons : Saturne II [13,14] at Saclay (up to 3 GeV), the KEK PS [37] at Tsukuba (up to 7 GeV), the ZGS [12] at Argonne (up to 12 GeV) and the AGS [15] at Brookhaven (up to 22 GeV). The most successful one is Saturne where proton and also deuteron polarized beams are routinely accelerated and used by the physicists. The highest energy (22 GeV) has been reached at the AGS and seems to be the limit of the present technology, beyond which new provisions are needed to counteract large depolarization due to the crossing of numerous and strong spin resonances. One generally considers the use of "Siberian snakes" which, in an experiment [38,39] at the Indiana University Cyclotron Facility (IUCF) Cooler Ring, have been shown to be efficient in suppressing depolarization on spin resonances.

At Saturne II, $2 \cdot 10^{11}$ particles per burst, either protons or deuterons, delivered by a polarized source with 90% polarization, are first injected and accelerated in the Mimas booster up to 47 MeV. Then they are extracted and injected in the main ring where they are accelerated up to the top energy. At injection in the rings the beam polarization is vertical. During acceleration the spin tune increases with the energy linearly. (See Eq. (18)). Spin resonances are crossed when the spin tune fulfills one of the conditions given by the Eq. (24). In the booster the vertical betatron tune Q_z must be set at a high value (2.48) to avoid the intrinsic resonance $\nu = 4 - Q_z$ even in the presence of a large tune shift due to space charge effect at injection. In the main ring, depending on the extraction energy, at most 15 resonances are crossed (Fig. 8). Special provisions are made to avoid depolarization at the resonance crossings, as described below. The net effect is only a spin reversal for some of these resonances. At the maximum energy of 3 GeV the overall depolarization during the complete cycle of acceleration is less than 15% as measured by a high-energy polarimeter.

At the AGS (Fig. 9), a polarized source has been used to deliver a $25 \mu\text{A}$ H^- beam with 75% polarization. This beam was first accelerated in a RFQ, then in a linac up to 200 MeV. After electron stripping through a thin carbon foil, the polarized proton beam was injected in the main ring. At the maximum energy of 22 GeV the proton beam ($2 \cdot 10^{10}$ ppp) was extracted and transported to the experimental area to bombard a polarized proton target in an experiment to measure the spin dependence of the proton-proton interaction.

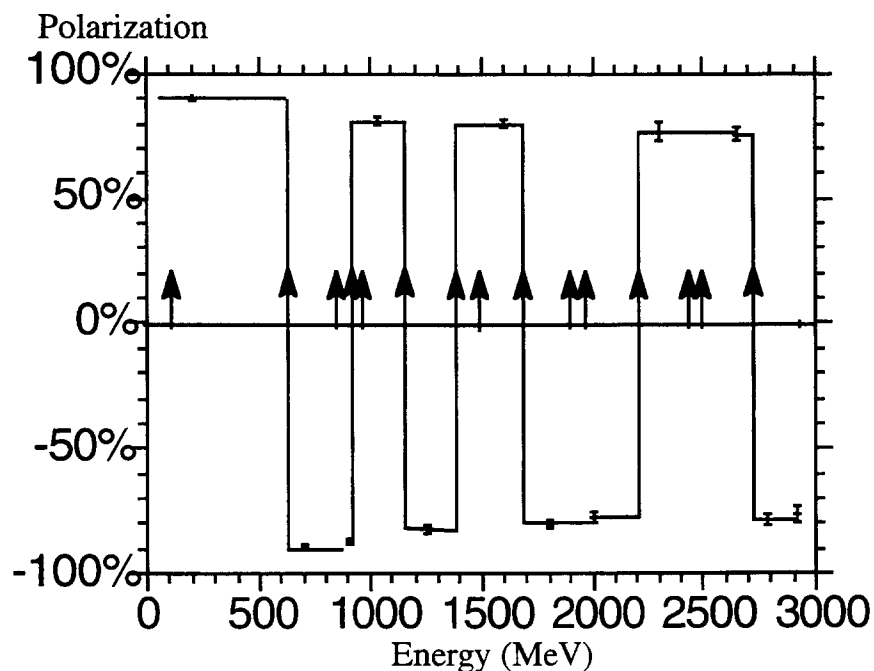


Fig. 8: The vertical polarization as function of the proton kinetic energy during the acceleration cycle in Saturne II [13,14]. The points with error bars are the experimental data. The arrows show the locations of the spin resonances. The solid line is a hand-drawn line showing the spin flips at the crossings of seven resonances.

The polarization was measured by polarimeters at several stages of the acceleration process : downstream of the linac before injection in the ring, inside the ring, and after extraction. During the acceleration cycle, one had to overcome 45 strong spin resonances to maintain the polarization up to 22 GeV, making the commissioning of the proton polarized beam a painstaking effort. The depolarization on the resonances is minimized using 95 dipole correctors and 12 pulsed quadrupoles. The obtained maximum polarization was 45% above a beam momentum of 16 GeV/c (Fig. 10).

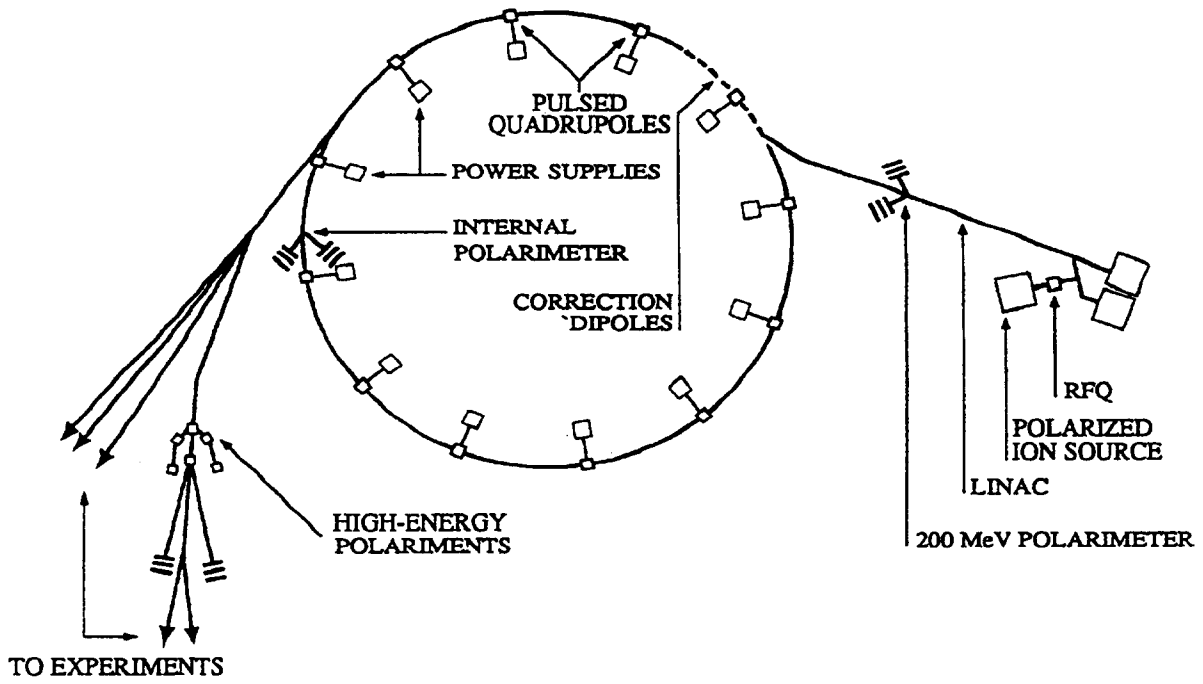


Fig. 9: The AGS [15] lay-out for the acceleration of polarized protons.

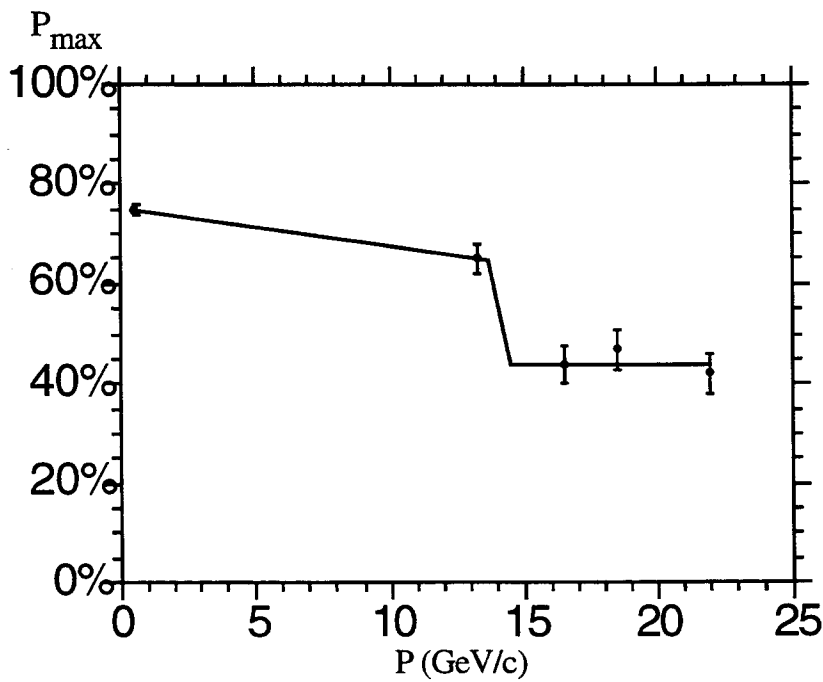


Fig. 10: The maximum AGS beam polarization [15] as function of the beam momentum showing a sharp polarization loss near 14 GeV/c.

3.2 Resonance crossing in proton synchrotrons

As the beam polarization must be maintained vertical to approach spin transparency, only the projection P_z of the polarization vector along the vertical line is considered. Any depolarization is measured as a decrease of the vertical projection. The spin resonances responsible for the most important vertical depolarization are of two types :

- The vertical betatron or intrinsic resonances (section 2.4.4.1) at spin tune values:

$$\nu = kp \pm Q_z$$

where p is the superperiodicity of the ring assumed to be perfect and k is any integer. When taking into account the ring imperfections, the superperiodicity is broken by the defects. Weaker resonances appear where kp becomes any integer.

- The synchrotron or imperfection resonances (section 2.4.4.3) at spin tune values:

$$\nu = k \pm Q_s$$

In most of the synchrotrons the synchrotron tune Q_s is much less than one. In the spectrum of spin resonances there are two synchrotron lines on both sides of each integer k . The most harmful imperfection resonances are those for which $k = np \pm m$ where n is any integer and m is an integer close to Q_z .

For imperfection resonances, the resonance strength ε scales linearly with the amplitude of the vertical closed-orbit and with the total proton energy (see Eq. 38). It lies in the 10^{-3} - 10^{-5} range at the AGS. For the intrinsic resonances the strength scales linearly with the energy and with the square root of the vertical emittance, lying in the 10^{-3} - 10^{-2} range.

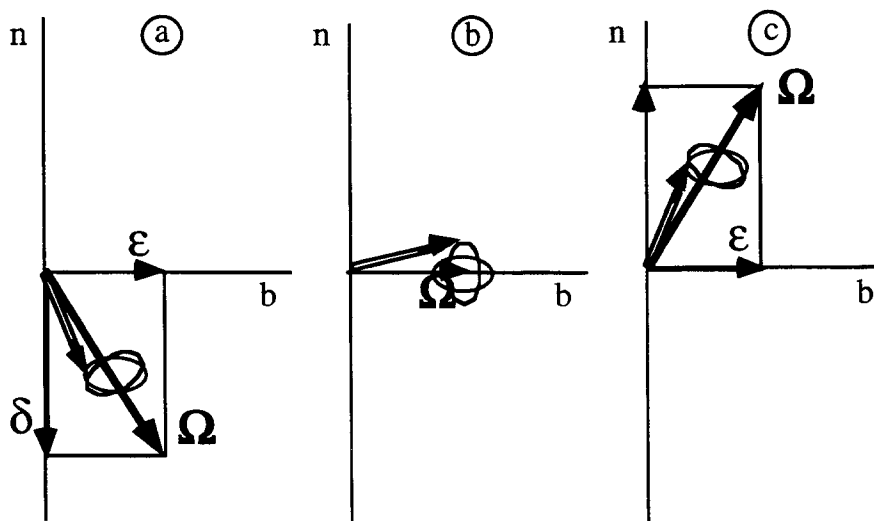


Fig. 11: The spin rotation as seen in the rotating frame near an isolated resonance. The rotation vector is Ω with components ε along the driving field \mathbf{b} and δ along the direction \mathbf{n} :

- a) below the resonance ($\delta < 0$),
- b) on top of the resonance ($\delta = 0$),
- c) above the resonance ($\delta > 0$).

During the acceleration cycle the spin tune ν increases monotonically and successively crosses several spin resonances. The width of the resonances, also measured by ε , is usually smaller than the resonance spacing. The resonances can be considered as if they would be isolated during their crossing. As in the general study of spin resonances (Section 2.4.1) the best way to study the spin perturbation when crossing a resonance is to consider a rotating frame. The only difference with the $(\mathbf{l}, \mathbf{m}, \mathbf{n})$ frame, used in Section 2.4.1, is that here this frame rotates about \mathbf{m} at the frequency ν_r of the resonant perturbing field instead of the frequency ν of the spin precession. With respect to this frame the perturbing field is at rest. The spin vector \mathbf{S} rotates about \mathbf{n} at the frequency $\delta = \nu - \nu_r$ and about \mathbf{b} at the frequency ε . Its overall rotation vector $\mathbf{\Omega}$ has components δ along \mathbf{n} and ε along \mathbf{b} (see Fig. 11). Far below the resonance, δ is negative and much larger than ε ; $\mathbf{\Omega}$ is nearly antiparallel to \mathbf{n} . When approaching the resonance, $\mathbf{\Omega}$ starts to move into the direction of \mathbf{b} . On top of the resonance, $\mathbf{\Omega}$ is exactly along \mathbf{b} . Above the resonance, $\mathbf{\Omega}$ now moves into the direction of \mathbf{n} and becomes nearly parallel to \mathbf{n} far above the resonance. The resonance crossing leads to a complete reversal of the rotation vector $\mathbf{\Omega}$.

The speed of the resonance crossing is measured by the rate α of the spin tune variation:

$$\nu = \nu_r + \alpha\theta \quad (43)$$

where θ is the azimuthal angle of the particle along the ring circumference. The "time" $\Delta\theta$ of the crossing is the width ε of the resonance divided by the rate α : $\Delta\theta = \varepsilon/\alpha$. During that time the rotation angle of the spin about \mathbf{b} is: $\psi = \varepsilon\Delta\theta = \varepsilon^2/\alpha$. There are two extreme regimes of resonance crossing:

- Fast crossing ($\psi \ll 1$): either the resonance is too narrow or the crossing rate is very large. There is not enough time to bend the spin vector away from the direction \mathbf{n} and there is no depolarization.
- Slow crossing ($\psi \gg 1$): either the resonance is very broad or the crossing rate is very slow. The spin vector rotates much faster about the rotation vector $\mathbf{\Omega}$ than the latter moves. The spin vector adiabatically follows the vector $\mathbf{\Omega}$ in its motion and undergoes a complete reversal as $\mathbf{\Omega}$. After the crossing the vertical polarization has changed sign, but there is no depolarization.

Between these two extreme regimes of crossing there is a partial spin flip. The decrease of the vertical component S_z of the spin vector is quantitatively given by the Froissart-Stora Formula [4]:

$$\frac{S_z^{\text{final}}}{S_z^{\text{initial}}} = 2 \exp\left(-\frac{\pi\varepsilon^2}{2\alpha}\right) - 1 \quad (44)$$

that also includes the two extreme regimes of fast crossing and adiabatic spin flip. The width ε of a resonance depends on the oscillation amplitude of the considered particle. A large

amplitude may lead to complete spin reversal. On the other hand, very small amplitudes do not cause significant change of S_z . To obtain the decrease of the vertical beam polarization P_z , i.e. the depolarization, one must average the Froissart-Stora formula over the particle amplitudes.

The adiabatic spin flip has been observed at Saturne at the crossing of five imperfection resonances and of two intrinsic resonances. Figure 12 shows detailed measurements [40] of the vertical polarization showing the spin flip when the beam is slowly extracted in the vicinity of the imperfection resonance $\gamma a = 3$.

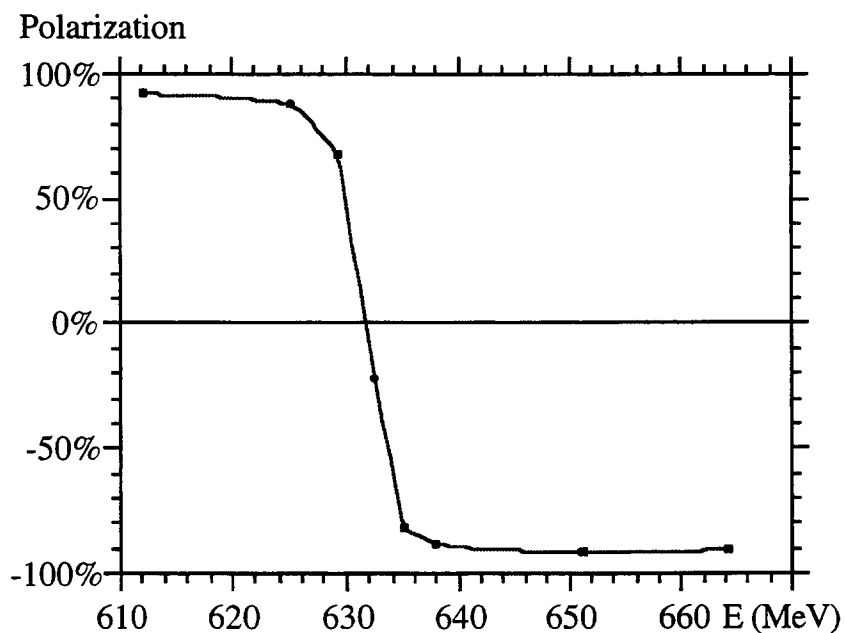


Fig.12: The vertical polarization P_z as function of the kinetic proton energy E , measured after slow extraction in the close vicinity of the imperfection resonance $\gamma a = 3$ ($E = 632$ MeV) at Saturne II [40].

Two different methods have been applied to avoid depolarization at the crossing of resonances that are not strong enough to obtain a complete spin flip :

- Compensation of the resonance strength ε (named also harmonic spin matching) : with some dipole correctors one can control the harmonics of the vertical closed-orbit distortion that drive an imperfection resonance. After a careful closed-orbit correction which minimizes the deviations of \mathbf{n} from the vertical, one maximizes the polarization, measured with a polarimeter, by adjusting the dipole correctors. This method has been successfully applied [15] to compensate about 35 imperfection resonances at the AGS using 95 correctors (Fig. 13).
- The same method using dipole correctors is also applied at Saturne II [13,14] to compensate the imperfection resonance $\gamma a = 2$. Similarly some intrinsic resonances are compensated using quadrupolar correctors.

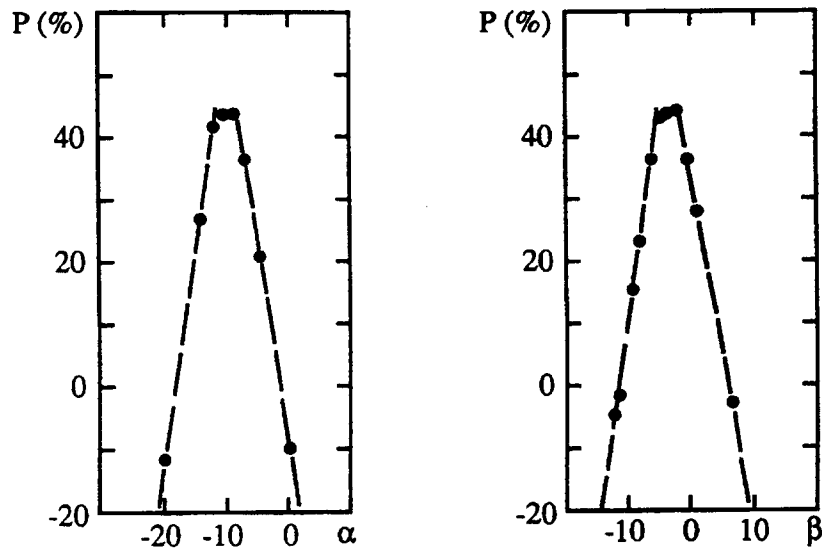


Fig. 13: The vertical polarization as function of the amplitudes α and β of the sine and cosine (resp.) harmonics that compensates the strong imperfection resonance $\gamma a = 9$ at the AGS [15].

- Speed increase of resonance crossing (also named resonance jumping) : when approaching an intrinsic resonance during acceleration, the vertical betatron tune is abruptly varied such that the resonance is crossed more rapidly (Fig 14). Thereafter the initial tune is slowly restored. At the AGS ten pulsed quadrupoles have been used to jump seven intrinsic resonances. The betatron tune was lowered by 0.25 with a $1.6 \mu\text{s}$ risetime and a $20 \mu\text{s}$ falltime.

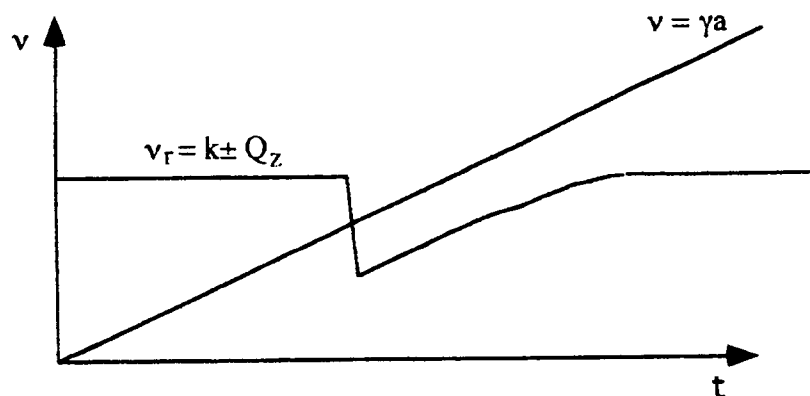


Fig. 14: Variation with time of the spin tune ν and of the tune ν_r of an intrinsic resonance, when the vertical betatron tune Q_z is rapidly shifted.

3.3 Siberian snakes

The number and the strengths of the spin resonances, crossed during the acceleration cycle, increase with energy. To accelerate polarized protons at the AGS up to 22 GeV a considerable effort has been required to overcome depolarization with the preceding methods when crossing 45 strong spin resonances. It would become unpractical at higher energies. A long time ago Ya. Derbenev and A. Kondatrenko [33,34] proposed to equip rings with special magnet arrangements, later named "Siberian snakes", that would avoid the crossing of all the resonances. With them the fractional spin tune becomes equal to $1/2$ and independent of energy. During acceleration the spin tune stays constant and never crosses tune values of spin resonances.

In principle a Siberian snake rotates any spin vector \mathbf{S} by π about an axis \mathbf{u} lying in the horizontal plane of the ring. In a ring equipped with one Siberian snake, the spin closed solution $\mathbf{n}(s)$ lies in the horizontal plane, apart inside the magnets of the Siberian snake. Figure 15 shows the motion of $\mathbf{n}(s)$ and of a spin vector \mathbf{S} . At the point 0, opposite to the snake, $\mathbf{n}(0)$ is parallel to the axis \mathbf{u} . Its direction $\mathbf{n}(\pi R)$ at the snake entrance is rotated into $\mathbf{n}'(\pi R)$ at the exit. The motion of $\mathbf{n}(s)$ before and after the snake are symmetric, such that $\mathbf{n}(s)$ again becomes parallel to the axis \mathbf{u} after one turn. The motion of another spin vector \mathbf{S} is also symmetric before and after passing through the snake. In particular at the point 0 its directions at the beginning and at the end of one turn are symmetric. Therefore they are connected by a rotation about the axis \mathbf{u} showing that the spin tune is effectively $1/2$ (the spin tune is the rotation angle in units of 2π).

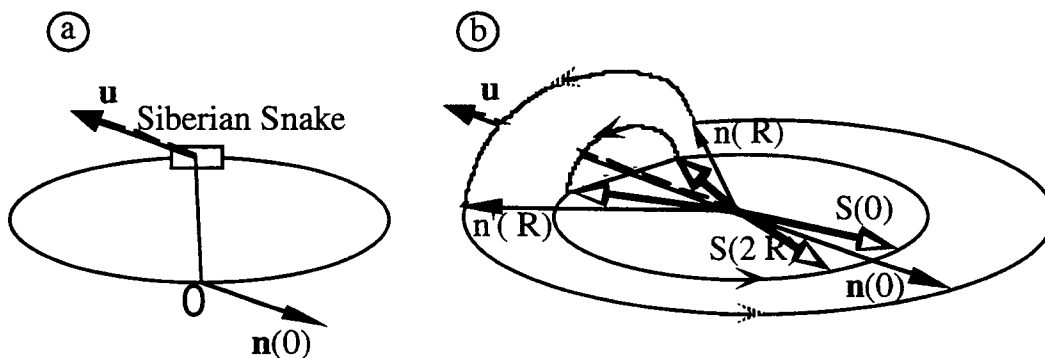


Fig. 15: a) A ring equipped with a Siberian snake located at $s = \pi R$. Its axis \mathbf{u} lies in the horizontal plane. The spin closed solution $\mathbf{n}(0)$ is parallel to \mathbf{u} at the origin 0 , opposite to the snake.
 b) Horizontal precession of the spin closed solution $\mathbf{n}(s)$ and of a spin vector \mathbf{S} lying in the ring plane. $\mathbf{n}(\pi R)$ and $\mathbf{n}'(\pi R)$ are the directions of $\mathbf{n}(s)$ at the entrance and at the exit of the snake respectively. $\mathbf{S}(0)$ and $\mathbf{S}(2\pi R)$ are the directions of the spin vector at the beginning and at the end of one turn respectively. The circles show the tracks of these vectors in the horizontal plane and about the snake axis \mathbf{u} .

The polarization behavior in a ring equipped with a snake is similar to the spin echo phenomenon used in NMR techniques. In a simple spin echo experiment a nuclear magnetic substance is magnetized and its magnetization vector \mathbf{M} precesses about a stationary magnetic field \mathbf{B}_0 perpendicular to \mathbf{M} (Fig. 16). Due to local field inhomogeneities, the magnetic moments \mathbf{u} of different nuclei precess at slightly different frequencies. If they were initially aligned in the same direction, they rapidly spread out and magnetization decreases. At time T a transient field is applied which rotates all the magnetic moments μ by π about the axis \mathbf{u} . The fastest moments which were in advance before the time T become the latest after that π rotation. At time $2T$ all the magnetic moments are again aligned together and the initial magnetization is restored. The spin vectors of the particles in a polarized beam are similar to the nuclear magnetic moments. They precess about the magnetic field of the ring bending magnets. The polarization vector \mathbf{P} is the analogue of the magnetization \mathbf{M} . The snake plays the role of the transient field and the spin-orbit coupling plays the role of the field inhomogeneities. The polarization decreases in the half turn preceding the snake and is restored at the end of the following half turn.

Generally one considers two kinds of Siberian snakes [34,41]. A snake of type I rotates the spin by π about an axis parallel to the reference orbit. At low momentum p (Gev/c) it can be made of a single solenoid with a field integral of $3.752xp$ (Tm) according to the Formula (13). A snake of type II rotates the spin by π about an axis perpendicular to the reference orbit. At high energies all kinds of snake would be made by sandwiches of several horizontally and vertically bending magnets, eventually combined into helical magnets.

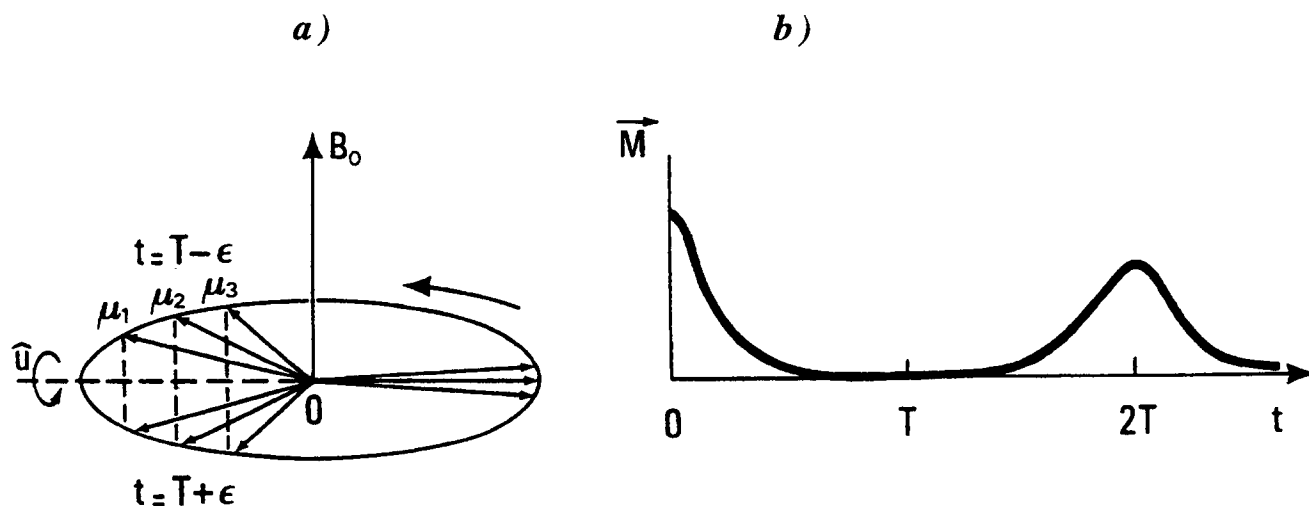


Fig. 16: Scheme of a NMR spin echo experiment :

- a) Precession of three magnetic moments $\mu_{1,2,3}$ about the magnetic field \mathbf{B}_0 with π rotation at time T . (Positions at times $T-\epsilon$ and $T+\epsilon$ are shown).
- b) The variation of the magnetization \mathbf{M} with time t .

The first experimental test [38,39] of a Siberian snake to overcome depolarizing resonances was made at the Indiana University Cyclotron Facility (IUCF) Cooler Ring. A type-I Siberian snake, made of a superconductive solenoid and correcting quadrupoles, was

installed in the Cooler Ring. Other solenoids were used to produce a variable longitudinal field operating as a controlled defect driving imperfection resonances. Proton beams were injected and stacked in the ring with either vertical or horizontal polarization to match the direction of the spin closed solution \mathbf{n} (vertical when the snake is off and horizontal when the snake is on). An internal polarimeter measured the vertical and radial components of the polarization. Fig. 17 shows the polarization data in the vicinity of the imperfection resonance $\gamma a = 2$ and the intrinsic resonance $\gamma a = -3 + Q_z$. For the imperfection resonance the proton beam energy was fixed at 104 MeV (4 MeV below the top of the resonance) and the field integral of the imperfection solenoids was varied. With the snake off, the vertical polarization was consistent with zero except when the defect field integral was nearly vanishing. On the contrary, with the snake on, the measured radial polarization was independent of the defect and close to its expected maximum. For the intrinsic resonance the proton beam energy was held to 177 MeV and the vertical betatron tune Q_z was varied. With the snake off, the vertical polarization was found to fall to zero for tune values close to the resonance, while radial polarization was maintained at its maximum for all tune values when the snake was turned on. In another test the vertical tune was ramped in a way equivalent to an energy ramping across the intrinsic resonance. With the snake off, the resonance crossing led to 75% polarization loss, but no observable depolarization with the snake turned on, proving the ability of Siberian snakes to overcome depolarization during acceleration. This positive result opens the possibility to accelerate polarized proton beams at higher energies than the AGS.

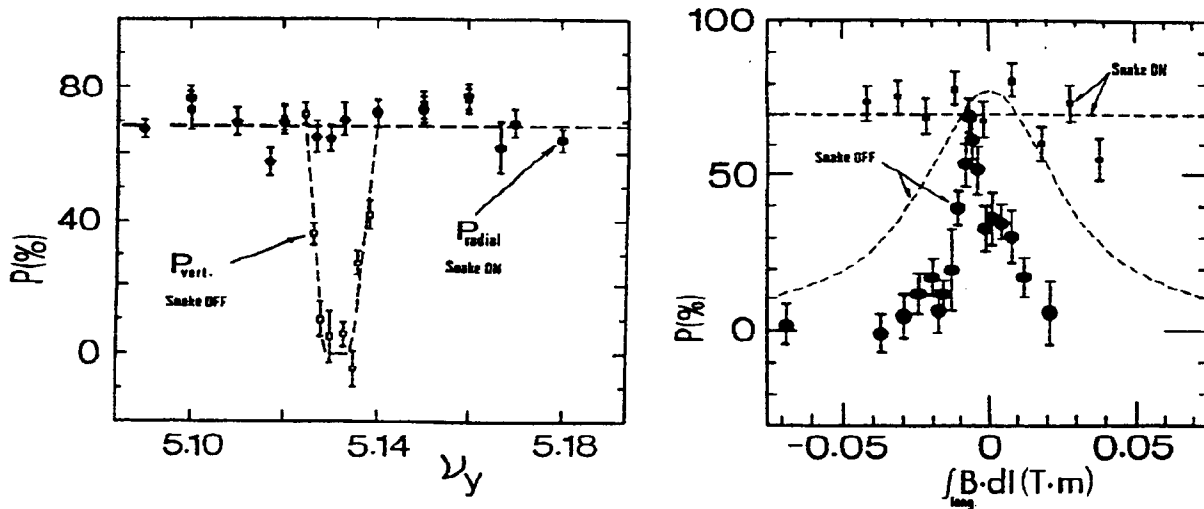


Fig. 17: Polarization data at the IUCF Cooler Ring [38,39] with a Siberian Snake. The vertical and the radial polarizations are measured when the snake is respectively turned off and on :

- At 177 MeV near the intrinsic resonance $\gamma a = -3 + Q_z$, varying the vertical betatron tune Q_z .
- At 104 MeV near the imperfection resonance $\gamma a = 2$, varying the field integral of the imperfection solenoids.

4. POLARIZATION OF ELECTRONS IN STORAGE RINGS

The orbital dynamics of electron and proton beams in high-energy storage rings are very different. Because of their much smaller mass, the electrons, subject to the central acceleration of the guide field, radiate energy. The quantum fluctuations associated with the photon emissions introduce a noise in the orbital motion. Conversely, the replacement of the lost energy by the RF cavities and differential radiation effects cause a damping of the excited orbital motion. The combination of the two effects determines the electron beam emittance, while the emittance of a proton beam depends on its value at injection.

Similarly, the dynamics of polarization are totally different. A polarized source must be used to inject polarized protons and the final polarization is at most equal to its initial value. Electrons become transversely polarized by a quantum mechanical effect which occurs when synchrotron photons are emitted. Conversely, the noise which perturbs the electron dynamics causes a diffusion of the spins. These two processes compete and lead to an equilibrium polarization.

4.1 Spontaneous polarization of the electrons

4.1.1 Spin-dependent synchrotron radiation

Ternov, Lostukov and Korovina [6] discovered that the probability for an electron to emit a photon depends slightly on the initial spin state of the electron. Sokolov and Ternov [7], by solving the Dirac equation in an homogeneous magnetic field, worked out the complete formula giving the rate of photon emission for an electron with given initial and final spin states in the direction of the magnetic field.

$$w(s_i, s_f) = \left(\frac{5\sqrt{3}}{6} \frac{e^2}{\hbar c} \frac{c}{\rho} \frac{E}{m_0 c^2} \right) \left[\begin{array}{l} \left(\text{if } s_i = s_f \right) \left\{ 1 - \frac{16\sqrt{3}}{45} \xi_0 + \frac{25}{18} \xi_0^2 - \frac{s_f}{5} \left(1 - \frac{20\sqrt{3}}{9} \xi_0 \right) \xi_0 \right\} \\ \left(\text{if } s_i \neq s_f \right) \left\{ \frac{1}{6} \left(1 - s_f \frac{8\sqrt{3}}{15} \right) \xi_0^2 \right\} \end{array} \right] \quad (45)$$

where ξ_0 is the ratio of the critical photon energy $\hbar\omega_c$ to the electron energy E . It is in general a very small value, e.g. 10^{-6} in LEP at 45 GeV. This formula shows that the vast majority of photon emissions does not involve spin flip. It is amusing to note that the beam radiates slightly less if it is polarized! The message of formula (45) is clarified by forming the asymmetries:

Spin flip versus non-spin flip events, whatever the spin state:

$$\frac{(w_{\uparrow\uparrow} + w_{\downarrow\downarrow}) - (w_{\uparrow\downarrow} + w_{\downarrow\uparrow})}{(w_{\uparrow\uparrow} + w_{\downarrow\downarrow}) + (w_{\uparrow\downarrow} + w_{\downarrow\uparrow})} = \frac{\xi_0^2}{3} \approx 10^{-12} \quad (46)$$

Dependence on the final spin state for spin flip events:

$$A = \frac{(w_{\uparrow\downarrow} - w_{\downarrow\uparrow})}{(w_{\uparrow\downarrow} + w_{\downarrow\uparrow})} = \frac{8}{5\sqrt{3}} \approx 0.924 \quad (47)$$

The probability for a spin flip is indeed very small. In case of a spin flip however, the preference for the spin state which is antiparallel to the magnetic field is almost one. There is thus a mechanism which forces the electron spins to the same state. A stored positron beam becomes polarized as well as an electron beam. However, the direction of polarization is opposite, i.e. parallel to the magnetic field. It is worth noting that in both cases the direction of polarization corresponds to a minimum of the magnetic energy (3). However, it has been shown that it is more a coincidence than a real cause [42].

4.1.2 Build-up of the polarization

In the uniform magnetic field we consider, the depolarizing effects are absent if one neglects the very small electron recoil. The dynamics of the polarization may thus be calculated from (45). At any given time, the beam polarization and its time derivative are given by:

$$P = \frac{N_{\uparrow} - N_{\downarrow}}{N} \quad \frac{dP}{dt} = \frac{1}{N} \left(\frac{dN_{\uparrow}}{dt} - \frac{dN_{\downarrow}}{dt} \right) \quad (48,49)$$

where N_{\uparrow} and N_{\downarrow} denote the number of electrons in each spin state. Their rate of change may easily be deduced from the transition probabilities (45):

$$\frac{dN_{\uparrow}}{dt} = N_{\downarrow}w_{\downarrow\uparrow} - N_{\uparrow}w_{\uparrow\downarrow} = Nw_{\downarrow\uparrow} - N_{\uparrow}(w_{\uparrow\downarrow} + w_{\downarrow\uparrow}) \quad (50)$$

and a similar expression for dN_{\downarrow}/dt . Replacing in (49) and integrating yields an exponential law for the growth of the polarization:

$$P = A(1 - e^{-t/\tau_p}) \quad (51)$$

The maximum degree of polarization is equal to the asymmetry A , i.e. 92.4%. Under very special circumstances, it has been shown [43] that the ultimate degree of polarization would reach 99.2% due to the contribution arising from the electron recoil in the photon field in the vicinity of a vertical betatron spin resonance. This enhancement of the polarization has not been observed so far.

The characteristic time τ_p of the polarization build-up is given by :

$$\tau_p^{-1} = (w_{\uparrow\downarrow} + w_{\downarrow\uparrow}) = \frac{5\sqrt{3}}{8} c\lambda_c r_e \frac{\gamma^5}{\rho^3} \quad (52)$$

where r_e is the electron classical radius, λ_c is the Compton wavelength divided by 2π and ρ is the bending radius in the homogeneous magnetic field. The polarization time decreases very rapidly when the energy is increased. It is due to the very fast increase of radiation rate that counteracts the low probability of spin flip in photon emission (Fig. 18).

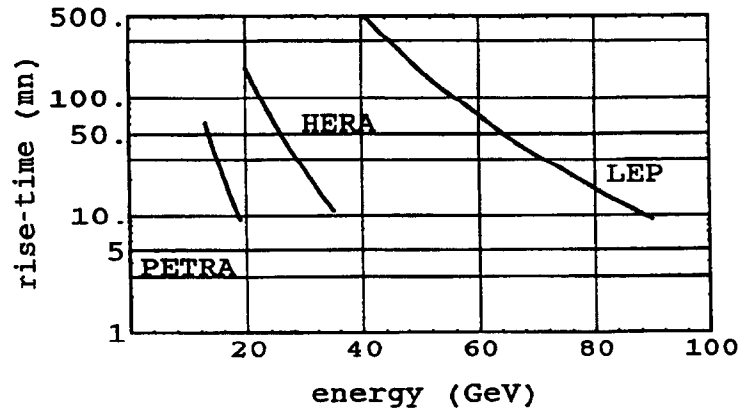


Fig. 18: Calculated polarization time versus energy for PETRA, HERA and LEP

4.1.3 Accelerator Guide Field

The guide field of real storage rings is in general piece-wise constant. It may in dipole insertions such as injection or wiggler magnets, change its strength or polarity. In this most common case, the expressions for the polarization level and rise-time can be generalized:

$$P_\infty = \frac{8}{5\sqrt{3}} \frac{\oint \rho^{-3} ds}{\oint |\rho^{-3}| ds} \quad (53)$$

$$\tau_p^{-1} = \frac{5\sqrt{3}}{8} c\lambda_c r_e \gamma^5 \frac{\oint |\rho^{-3}| ds}{\oint ds} \quad (54)$$

The difference with the uniform field case (47) (52) is in general negligible.

4.1.4 Experimental observations

The polarization build-up by the Sokolov-Ternov effect has been observed in all the electron storage rings where it has been sought. Table 2 gives the polarization data for some of these rings.

Table 2

Polarization experimental data for some electron storage rings. The time τ_p is the *theoretical* polarization time given by Eq.(54) at energy E . The polarization degree P is a typically *measured* value.

	VEPP[10]	VEPP2-M[11]	ACO[8,9]	BESSY[44]	SPEAR[45]	VEPP4[46]
$E(\text{GeV})$	0.640	0.625	0.536	0.800	3.70	5.0
$\tau_p(\text{min})$	50	70	160	150	15	40
$P(\%)$	52	90	90	>75	>70	80
	DORIS II[47]	CESR[48]	PETRA[49]	HERA[19]	TRISTAN[50]	LEP[51]
$E(\text{GeV})$	5.0	4.7	16.5	26.7	29	46.5
$\tau_p(\text{min})$	4	300	18	40	2	300
$P(\%)$	80	30*	80**	70**	75**	57**

Figure 19 shows the polarization build-up as function of time at 26.7 GeV in HERA, following closely equation (51). The fifth power law of the polarization time versus energy is observed when the beam energy is changed in a storage ring. In particular the polarization time at LEP becomes very long in the lower part of its energy range : five hours at the energy (46 GeV) of the Z_0 vector boson production. The polarization time also increases as the third power of ρ , explaining why several rings have different polarization times at the same energy.

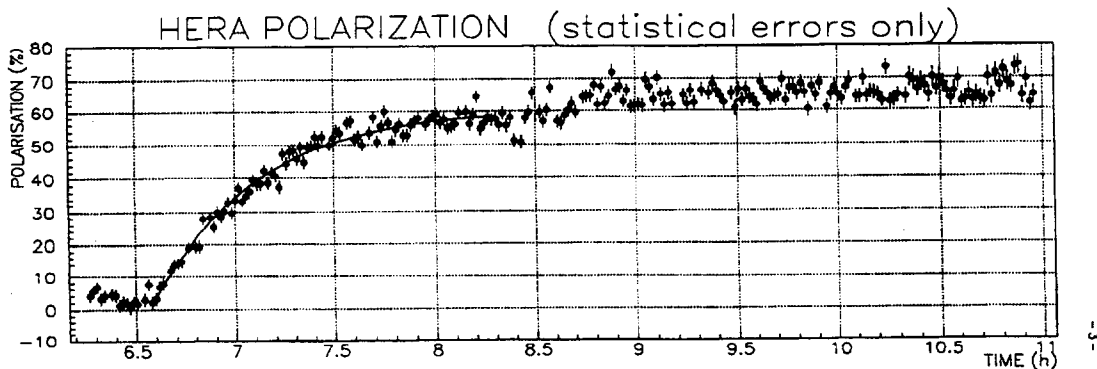


Fig. 19: Polarization P versus the time t in the storage ring HERA at 26.7 GeV.

The experimental values (see Table 2) indicate that the equilibrium polarization is in general lower than the theoretical 92.4% value, especially in multi-GeV rings.

4.1.5 Enhancement of the polarization build-up

* after 120 min.

** after harmonic correction (harmonic spin matching).

In CESR and LEP1, the design of the machine is such that the polarization time constant is as long as 5 hours. This is a serious drawback in practice: it takes a long time before the beams are highly polarized and empirical adjustments of the polarization are difficult given the long response time. It appears from formula (54) that it should be possible to reduce significantly the polarization rise-time by increasing locally the bending radius. This can be done with an asymmetric dipole wiggler as shown on figure 20.

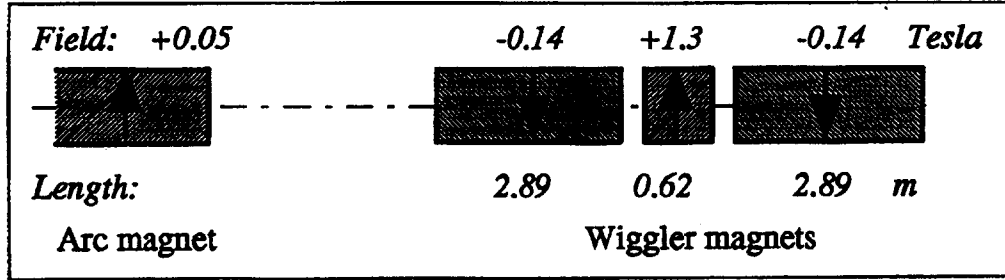


Fig.20: The LEP asymmetric wiggler to enhance the Sokolov-Ternov effect

The central part of the wiggler is designed with the highest magnetic field pointing in the direction of the main guide field; it is compensated on each side by the weakest field compatible with a reasonable magnet length. In this way, the asymptotic polarization level P_{∞} is hardly decreased (Eq.(53)) while the rise-time is drastically reduced. Such a scheme has been designed for LEP and successfully used to decrease the rise-time by a factor of 2 [51]. Beyond, the enhanced synchrotron radiation which increases the beam energy spread, causes other phenomena which depolarize the beam.

4.1.6 Non-uniform magnetic field

The results of Sokolov and Ternov for a uniform magnetic field were generalized to arbitrary field configurations by Baier, Katkov and Strakhovenko [52]. The expressions for the asymptotic polarization level and the polarization rise-time can be deduced [53, 54] provided the spin dynamics is not perturbed by spin resonances: the approximation is valid at low energy, for weak (compensated) spin resonances, for a spin tune far from resonances.

$$P_{\infty} = \frac{8}{5\sqrt{3}} \frac{\langle |\rho^{-3}| \mathbf{n} \cdot \mathbf{b} \rangle}{\langle |\rho^{-3}| \left[1 - \frac{2}{9} (\beta \cdot \mathbf{n})^2 \right] \rangle} \quad (55)$$

$$\tau_p^{-1} = \frac{5\sqrt{3}}{8} c \chi_r e \gamma^5 \langle |\rho^{-3}| \left[1 - \frac{2}{9} (\beta \cdot \mathbf{n})^2 \right] \rangle \quad (56)$$

The brackets $\langle \rangle$ stand for the average along the machine circumference; \mathbf{b} is the unit vector in the direction of the magnetic field of bending radius ρ . These formulae show that the useful component of the magnetic field is along \mathbf{n} , i.e. that \mathbf{n} is the equilibrium polarization direction.

In general, non-uniform magnetic fields give an asymptotic polarization lower than the maximum of 92.4%.

4.2 Resonant spin diffusion and equilibrium polarization

Equation (46) shows that, in the vast majority of the cases (6000 times per turn in LEP at 45 GeV), the photon emission is not associated with a spin flip. The sudden energy jump causes the electron to initiate additional synchrotron and betatron oscillations if the dispersion functions do not vanish at the azimuth of the photon emission. The resulting orbital motion is thus “noisy”, causing a diffusion eventually balanced by radiation damping along the perturbed trajectory. The spin experiences extra rotations and diffusion as well. The synchrotron and betatron oscillations are damped with a characteristic time (10^{-2} - 10^{-3} sec) much shorter than the polarization time of the Sokolov-Ternov effect (10^{+2} - 10^{+4} sec). It is thus legitimate to consider separately the spin diffusion due to the non-spin-flip events and the Sokolov-Ternov mechanism.

4.2.1 Ideal storage ring

In an ideally planar ring, only synchrotron and horizontal betatron oscillations are excited by the photon emission. The small vertical angle of the electron recoil at photon emission is totally negligible at high energy. The diffusion due to the quantum excitation results in equilibrium longitudinal and horizontal emittances. The particle motion being constrained to remain in the horizontal plane, the quantum excitation only causes stochastic spin precessions about the vertical axis; they are of no consequence as long as the spin is vertical, i.e. in the \mathbf{n} direction. (See Section 2.3.1) This is indeed the case if the polarization is due to the Sokolov-Ternov effect. This situation is different from a proton beam which has a finite vertical emittance and may be depolarized when crossing an intrinsic resonance even if there are no defects. (See Section 3.2) The only consequence of the quantum excitation is a partial randomization of the spin precession phases. The spin tune is defined by averaging over several turns.

4.2.2 Spin perturbation by quantum excitation

The general case is best explained by Figure 21. It shows the evolution of the phase space and spin coordinates of a reference particle which emits a photon. The first line represents the state of the particle just before the photon emission: the particle is at rest, at the origin of the coordinates, i.e. on the closed orbit; the spin is along \mathbf{n} assumed to be vertical.

The second line represents the state just after the photon emission: the energy coordinate suddenly became negative. The position of the particle could not change during the short photon emission. However, the break-down of the position into closed orbit, dispersion orbit and betatron amplitude does change if the dispersion function does not vanish. The momenta change due both to the photon emission and for the same reason as above. This causes the particle to start oscillating in the three phase planes. Along the new trajectory, the spin motion is slightly different, precessing about a new spin axis \mathbf{n} , in general tilted with respect to the initial spin direction.

The third line shows the evolution of the coordinates over a few damping times. The spatial and momentum coordinates are damped down by the well-known damping mechanism (see the CAS lecture on electron dynamics). As the trajectory gradually converges towards its unperturbed position, the spin axis \mathbf{n} is gradually restored to its initial vertical position. The particle spin however, which precesses very rapidly about it, follows adiabatically the \mathbf{n} axis and finds itself tilted at an angle when the orbital coordinates have been restored. The horizontal component of the spin precesses in a stochastic way as photons are emitted. Its average over all particles of the beam vanishes. The remaining polarization is the projection of the initial polarization vector onto the spin axis after it has been tilted by the photon emission. This rather simple picture of depolarization due to quantum excitation arises because of the very large difference between the time constants of the three relevant phenomena: $1 \mu\text{s}$ for one spin precession, 50 ms for the damping of the orbital coordinates and the gradual change of the \mathbf{n} axis, 5 hours for the Sokolov-Ternov polarizing mechanism (LEP at 45 GeV).

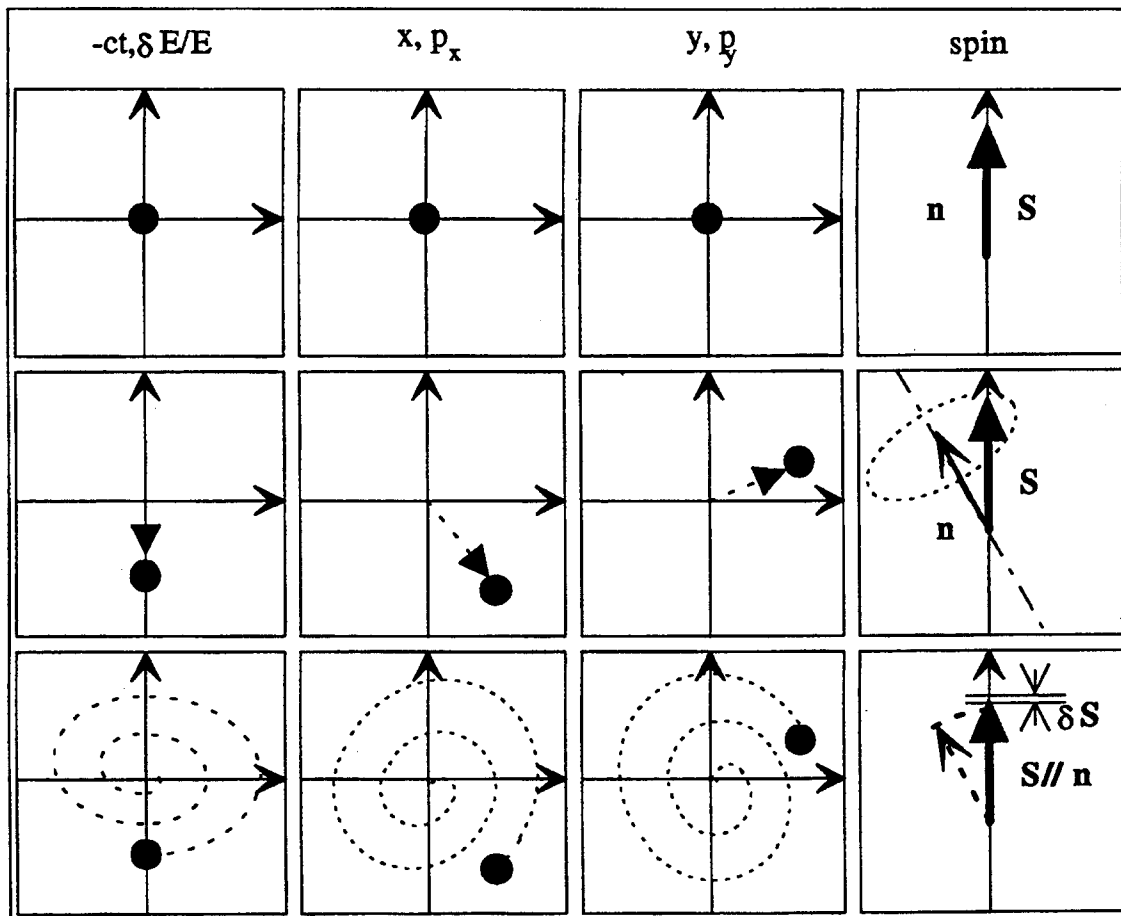


Fig. 21: Model of a quantum excitation

4.2.3 Spin diffusion and equilibrium polarization

This simple model of the spin diffusion process leads to a good estimate of the polarization level. Let us assume that the tilt $\delta \mathbf{n}$ of the \mathbf{n} axis just after the emission of photon of energy δE is proportional to the relative energy loss (Figure 21):

$$\delta \mathbf{n} = \mathbf{d}(s) \frac{\delta E}{E} \quad (57)$$

The proportionality constant $\mathbf{d}(s)$ is a vectorial quantity which depends on the azimuth. It summarizes the contributions from the horizontal and vertical betatron oscillations as well as from the synchrotron oscillation.

For a single energy jump the decrease of the polarization P along the spin closed solution \mathbf{n} is given by :

$$\frac{\delta P}{P} \approx \frac{1}{2} \left| \mathbf{d} \frac{\delta E}{E} \right|^2 \quad (58)$$

To combine in a simple way the effect of the many energy jumps we assume linearity of the orbital motion of the particles. In this case, which is generally a good approximation, the perturbations add up linearly in an incoherent way. As the times of photon emission and the energy jumps are random, the spin motion becomes a random process, i.e. diffuse away from the spin closed solution \mathbf{n} . Within the linear approximation the rate of the polarization decrease is obtained by summing the effects of all the successive energy jumps per unit time. The average rate $1/\tau_d$ of decrease of the spin component is found by averaging over the coordinate s and the energy jump δE :

$$\frac{1}{\tau_d} = \frac{1}{dt} \frac{\delta P}{P} \approx \frac{1}{2} N \left\langle \left| \mathbf{d} \frac{\delta E}{E} \right|^2 \right\rangle \quad (59)$$

where N is the photon emission rate and the brackets $\langle \rangle$ indicate the averaging. The quantity $N \langle (dE/E)^2 \rangle$ happens to be closely related to the polarization rise-time τ_p [55], yielding

$$\frac{\tau_p}{\tau_d} = \frac{11}{18} \langle |\mathbf{d}|^2 \rangle \quad (60)$$

When taking into account this depolarizing process Eq. (51) becomes:

$$P = P_\infty \left(1 - e^{-\frac{t}{\tau_p + \tau_d}} \right) \quad (61)$$

$$P_\infty = \frac{8}{5\sqrt{3}} \frac{1}{\left(1 + \frac{\tau_p}{\tau_d} \right)} = \frac{8}{5\sqrt{3}} \frac{1}{\left(1 + \frac{11}{18} \langle |\mathbf{d}|^2 \rangle \right)} \quad (62)$$

where the averaging $\langle \rangle$ is made over the azimuth s . The knowledge of $\mathbf{d}(s)$ is sufficient for a complete description of the polarization dynamics.

In a more thorough study of the equilibrium polarization Ya. Derbenev and A. Kondratenko [56] derived a formula for an arbitrary configuration of magnetic fields:

$$P_{\infty} = \frac{8}{5\sqrt{3}} \frac{\left\langle \left| \rho^{-3} \mathbf{b} \cdot \left(\mathbf{n} - \gamma \frac{\delta \mathbf{n}}{\delta \gamma} \right) \right| \right\rangle}{\left\langle \left| \rho^{-3} \left(1 - \frac{2}{9} (\boldsymbol{\beta} \cdot \mathbf{n})^2 + \frac{11}{18} \left| \gamma \frac{\delta \mathbf{n}}{\delta \gamma} \right|^2 \right) \right| \right\rangle} \quad (63)$$

where ρ is the bending radius, \mathbf{b} a unit vector along the transverse component of the field and $\boldsymbol{\beta}$ a unit vector along the reference orbit.

The vector \mathbf{n} is *no longer the spin closed solution attached to the closed orbit*. It is defined for any location or synchrotron trajectory as the solution of the BMT equation (11) which is quasi-periodic in the six-dimensional phase space, i.e. periodic in each angle variables and azimuth. The general \mathbf{n} vector reduces to the spin closed solution when evaluated on the closed orbit.

Comparing formulae (62) and (63), it appears that $\gamma \delta \mathbf{n} / \delta \gamma$, named the spin-orbit coupling vector, can be identified with the deviation vector \mathbf{d} of the simple diffusion model. The averaging in the Derbenev-Kondratenko formula (63) must be done over all six orbital coordinates since $\gamma \delta \mathbf{n} / \delta \gamma$ depends on oscillation phases and amplitudes, in addition to the averaging over the azimuth s . The $\gamma \delta \mathbf{n} / \delta \gamma$ linear term in the numerator of formula (63) usually gives a negligible contribution compared to the quadratic term in the denominator. The contributions of the electron recoil during photon emission, that have also been included in other calculations [57, 58], appear to be negligible at high energy.

The effective polarization rate in (61) is the sum of the Sokolov-Ternov rate τ_p^{-1} and of the depolarization rate τ_d^{-1} . Therefore in the presence of imperfections the polarization time τ is shorter than the ideal value τ_p . When the polarization time is too long to reach the equilibrium polarization, one can derive its value P_{eq} just by measuring the rate of increase of the polarization at the beginning and by using equation (61). It can also be used to calibrate in polarization degree the experimental data of a polarimeter (Fig. 22).

This analysis shows how different the polarized electrons and protons are. The spin motion of a proton is deterministic and beam depolarization results from the incoherent spread of trajectories and energies. For an electron the spin motion is random and beam depolarization results from the random quantum fluctuations of synchrotron radiation. Moreover, the electron beam depolarization is an irreversible process. On the contrary proton beam polarization can be restored. A Siberian snake is an example of polarization restore after one turn. That also explains why Siberian snakes are not efficient in overcoming depolarization in electron rings [59].

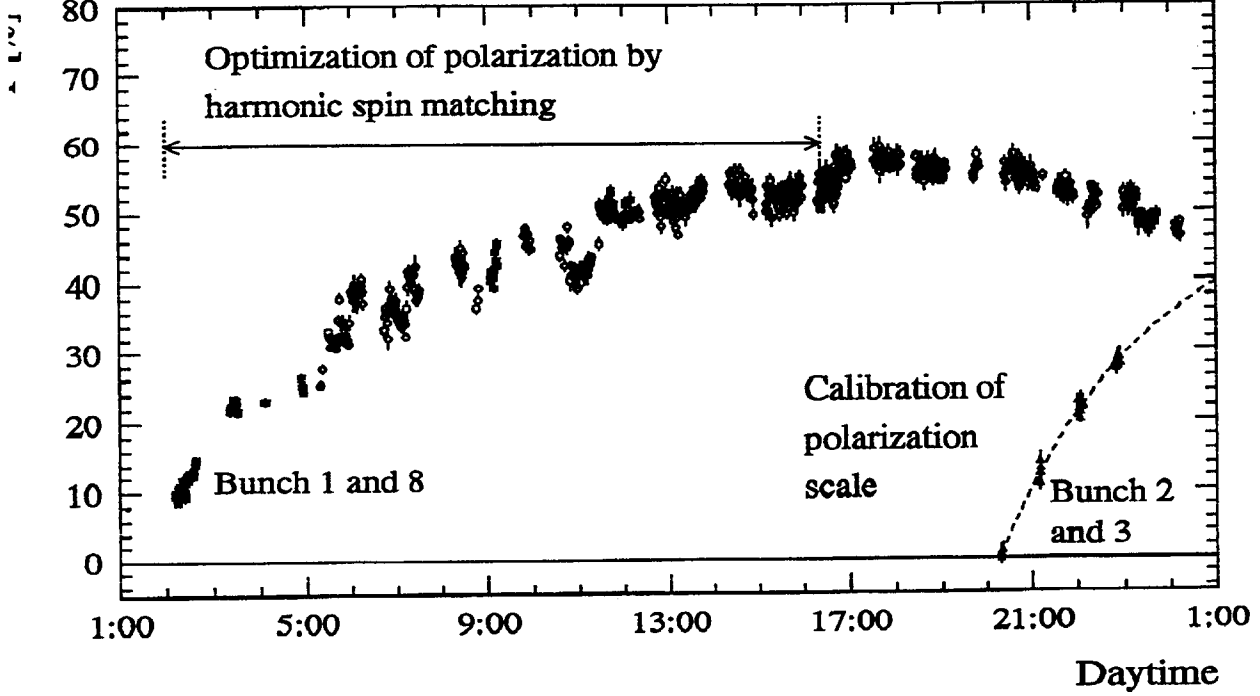


Fig. 22: Polarimeter data versus time at an energy of 46.55 GeV in LEP. The bunches 2 and 3 were selectively depolarized to allow the absolute calibration of the polarization scale [51]

4.2.4 Spin-orbit coupling in the linear approximation

In a small amplitude linear model of orbital motion, the result of the first-order calculation of the spin-orbit coupling vector $\mathbf{d}(s)$ is a linear combination of contributions from the three oscillations [60]:

$$\mathbf{d}(s) = \frac{1}{2} \text{Im} \left[(\mathbf{m} + i\mathbf{l})^* (\Delta_x + \Delta_{-x} + \Delta_z + \Delta_{-z} + \Delta_s + \Delta_{-s}) \right] \quad (64)$$

Each contribution can be expressed by the product of a resonant term with an integral over s of the coupling between the spin motion and the considered orbital oscillation.

$$\Delta_{\pm x, z}(s) = (1 + a\gamma) \frac{[-D \pm i(\alpha D + \beta D')]_{x, z}}{\sqrt{\beta_{x, z}}} \frac{1}{e^{2i\pi(\nu \pm Q_{x, z})} - 1} J_{\pm x, z}(s) e^{\mp i\phi_{x, z}} \quad (65)$$

$$\Delta_{\pm s}(s) = (1 + a\gamma) \frac{1}{e^{2i\pi(\nu \pm Q_s)} - 1} J_{\pm s}(s) e^{\mp i\phi_s} \quad (66)$$

where D and D' are the dispersion and its derivative, and $\phi_{x,z,s}$ the phases of the betatron and synchrotron oscillations. On resonance, the spin-orbit coupling vector $\mathbf{d}(s)$ becomes arbitrarily large in this linear approximation and the polarization vanishes according to (63). The condition is:

$$\nu = k \pm Q_{x,z,s}$$

corresponding to the linear resonances described in section 2.4.4. The real keys for controlling the polarization level are the spin-orbit coupling integrals $\mathbf{J}_{\pm x,z,s}(s)$, for, if they can be made to vanish, spin-transparency can be recovered, even close to the resonance conditions. These integrals already appeared in the expression of the resonance strengths (see Eq.(38)).

$$\begin{aligned} \mathbf{J}_{\pm z}(s) &= \int_s^{s+C} (\mathbf{m} + i\mathbf{l}) \cdot \mathbf{x} K \sqrt{\beta_z} e^{\pm i\phi_z} ds' \\ \mathbf{J}_{\pm x}(s) &= \int_s^{s+C} (\mathbf{m} + i\mathbf{l}) \cdot \mathbf{z} K \sqrt{\beta_x} e^{\pm i\phi_x} ds' \\ \mathbf{J}_{\pm s}(s) &= \int_s^{s+C} (\mathbf{m} + i\mathbf{l}) \cdot K(D_x z + D_z x) e^{\pm i\phi_s} ds' \end{aligned} \quad (67,68,69)$$

As already noted in section 2.4.3, $\mathbf{J}_{\pm x,s}(s)$ are sensitive to the tilt of the \mathbf{n} axis. The spin-orbit coupling vector $\mathbf{d}(s)$, just like the tilt of the closed spin solution \mathbf{n} , shows a large increase close to the integer resonances $\nu = k$

To summarize, the spin-orbit coupling vector $\mathbf{d}(s)$ becomes large on resonance, causing a significant reduction of the polarization. It scales linearly with energy. Its amplitude, for small oscillation amplitudes, is conveniently expressed in terms of the spin-orbit coupling integrals. There are several implementations of the calculation of $\mathbf{d}(s)$ and of the equilibrium polarization in the linear approximation. The most popular is SLIM [61]. Its approach is very elegant and has been widely used in many other codes. The limitations are mainly technical: SLIM assumes thin lenses and does not allow optics imperfections to be described in a natural way. The program SITF [62] integrates approximately the spin motion in thick elements. It allows for a complete description of optics errors, in the FORTRAN-like PETROS syntax. SITF was integrated as a module in MAD [63]. There it benefits from the powerful MAD language, which allows a natural and flexible description of the optics imperfections and, for example, of the harmonic orbit bumps. This powerful implementation has contributed to the success of the polarization program in LEP, largely based on calculations.

4.2.5 Spin-orbit coupling at higher orders

As the amplitudes of the betatron and synchrotron oscillations scale linearly with energy in a given machine, the assumption of vanishingly small oscillations is bound to break down at some energy and so does the analysis we performed, only considering the \mathbf{n} axis on the closed orbit. Qualitatively, we already saw in sections 2.4.5 and 2.4.6 that new resonance conditions emerge, both due to the influence of the non-linear fields, e.g. of the sextupoles, and to the FM modulation of the beam oscillations by the finite amplitude synchrotron motion. In addition, the spin-orbit coupling vector also increases linearly with energy. The spin resonances become wider and wider until their separation becomes comparable with their width. A run-away is expected at an energy threshold above which polarization would become practically impossible.

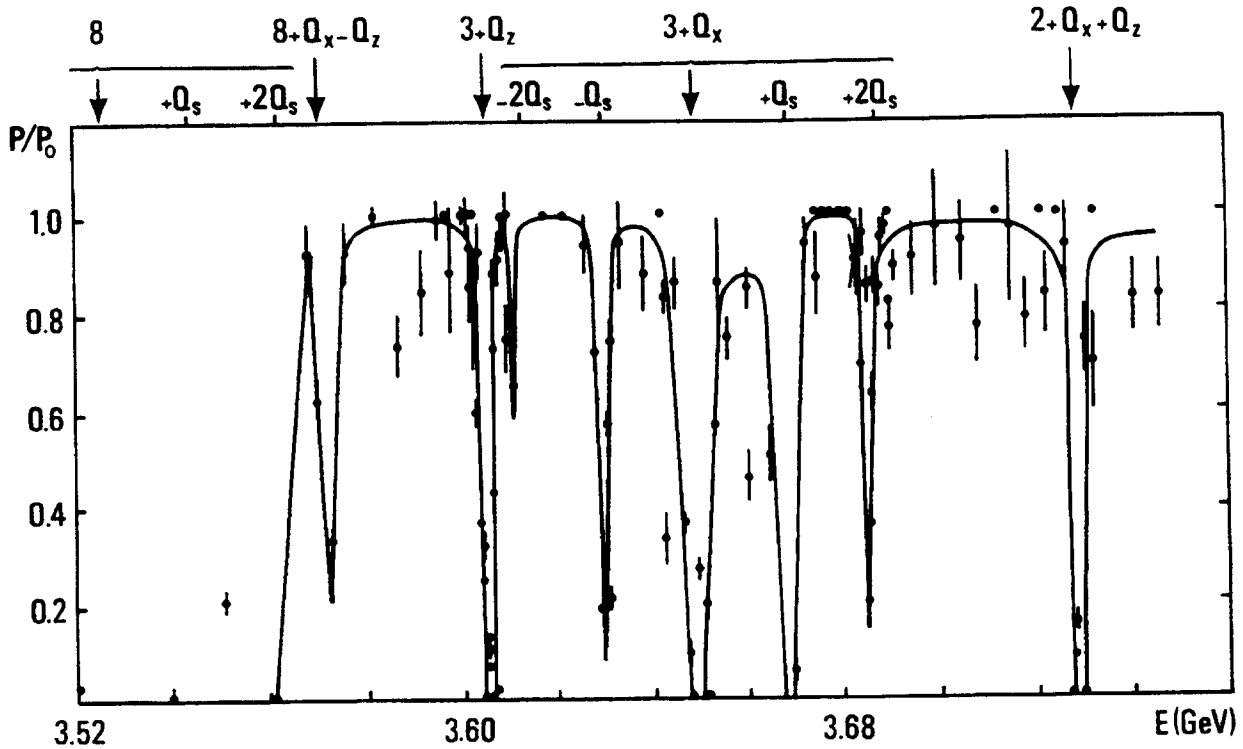


Fig.23: Relative polarization P/P_0 ($P_0 = 92.4\%$) versus beam energy at SPEAR [45]. The solid line is a hand-drawn line to guide the eye. The spin resonances labelled : $k + k_x Q_x + Q_z + k_s Q_s$ are indicated above the figure.

Figure 23 shows the most detailed scan of the polarization as a function of beam energy at the SPEAR storage ring[45]. It shows the depolarization on many spin resonances in a small energy interval, particularly near the synchrotron resonance $\gamma a = 8$ at 3.5 GeV. Despite the low energy, several non-linear and higher-order spin resonances appear harmful, particularly synchrotron satellites of the horizontal betatron resonance $\gamma a = 3 + Q_x$. This evidence, and some early calculations, left the impression that polarization might not be possible in HERA and LEP. Given the renewed interest in polarized beams, several attempts were made to calculate higher-order effects.

Several analytical approaches [64 and e.g. 65] have singled out the modulation index x as the relevant parameter for higher-order synchrotron effects:

$$x = \left(\frac{v \sigma_e}{Q_s E} \right)^2 \quad (70)$$

σ_e/E is the relative energy spread of the beam. The modulation index ranges from 3% in SPEAR to 50% in LEP at 46 GeV and about 200% in HERA at 27 GeV and in LEP with wigglers. The asymptotic polarization level can be estimated from an enhancement function $C(x)$ of the depolarization as given by formula (62):

$$P_{\infty} = \frac{8}{5\sqrt{3}} \frac{1}{1 + C(x) \frac{\tau_p}{\tau_d} \Big|_{x=0}} \quad (71)$$

$C(x)$ is a combination of Bessel functions encountered in FM modulation. It summarizes the contribution to the depolarization of the synchrotron satellites which surround each linear spin resonance. (See section 2.4.6) The amplification factor for the strongest synchrotron spin resonances is typically between 1 and 2 at HERA over its energy range and between 1.5 and 20 at 46 GeV at LEP depending on the wiggler excitation (Fig. 24).

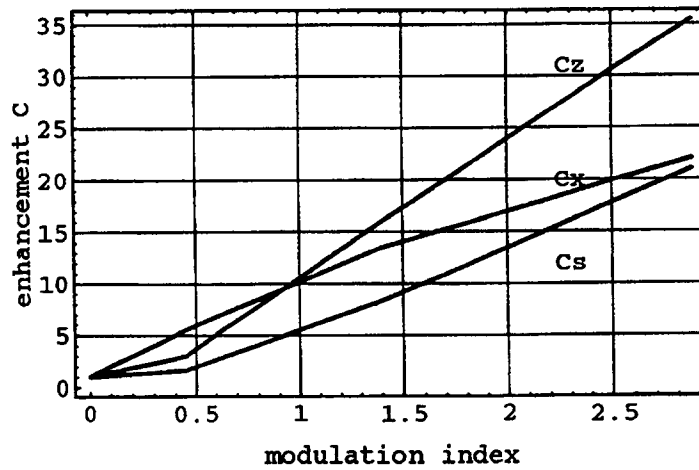


Fig. 24: Variation of the enhancement function with the modulation index in LEP [65]

The importance of the beam energy spread is confirmed by an experiment made at LEP where it was increased at constant energy (46 GeV) by means of asymmetric wiggler magnets (Fig. 25). The polarization level decreases with the beam energy spread, in agreement with calculations [51].

A purely analytical approach is limited to the calculation of the enhancement factor, i.e. of the relative strength of the synchrotron satellites. The full spectrum of the generic linear resonances must be calculated numerically. Various numerical or semi-numerical approaches have been carried out lately, all requiring heavy computations:

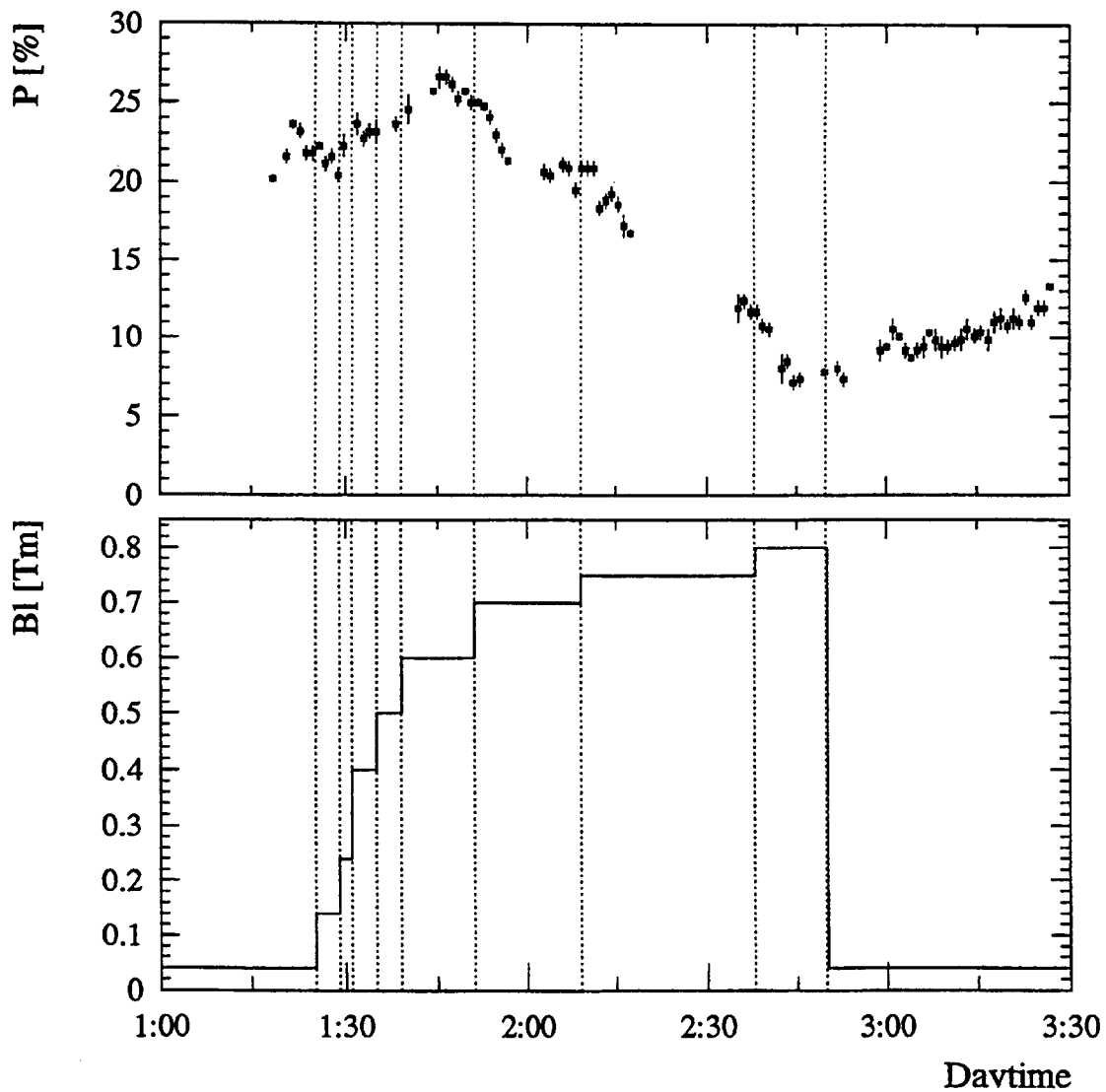


Fig. 25: Measured polarization as a function of beam energy spread at LEP [51], enhanced by a wiggler of strength $B \ell$

- SMILE [66] implements a recursive perturbative solution of the BMT equation, where the small parameters are taken to be the amplitudes of the oscillations. This program could predict the non-linear and higher-order spin resonances at relatively low energy (SPEAR at 3.6 GeV). However a critical analysis of its prediction for HERA (27 GeV) and LEP (46 GeV) showed that the very pessimistic results obtained were due to the non-convergence in the calculation of the synchrotron spin resonances at these energies. The program was modified to compute the latter using the analytical approach mentioned above. SMILE is available in a stand-alone version and as a module of the optics program MAD.

- SODOM [67] implements a non-perturbative approach. Advantage is taken from the known periodicities of the general \mathbf{n} -axis and of its transport around the machine to compute the most significant harmonics of \mathbf{n} . The variation of \mathbf{n} with respect to a finite energy difference yields its derivative $\gamma \delta \mathbf{n} / \delta \gamma$, allowing the computation of the equilibrium polarization level. The program is available in a stand-alone version and as a module of MAD [68]. Preliminary checks against measured higher-order depolarization phenomena in LEP (depolarization by an asymmetric wiggler, Fig. 25) and prediction of the strength of synchrotron satellite (Fig. 26) seem to validate this approach [51].

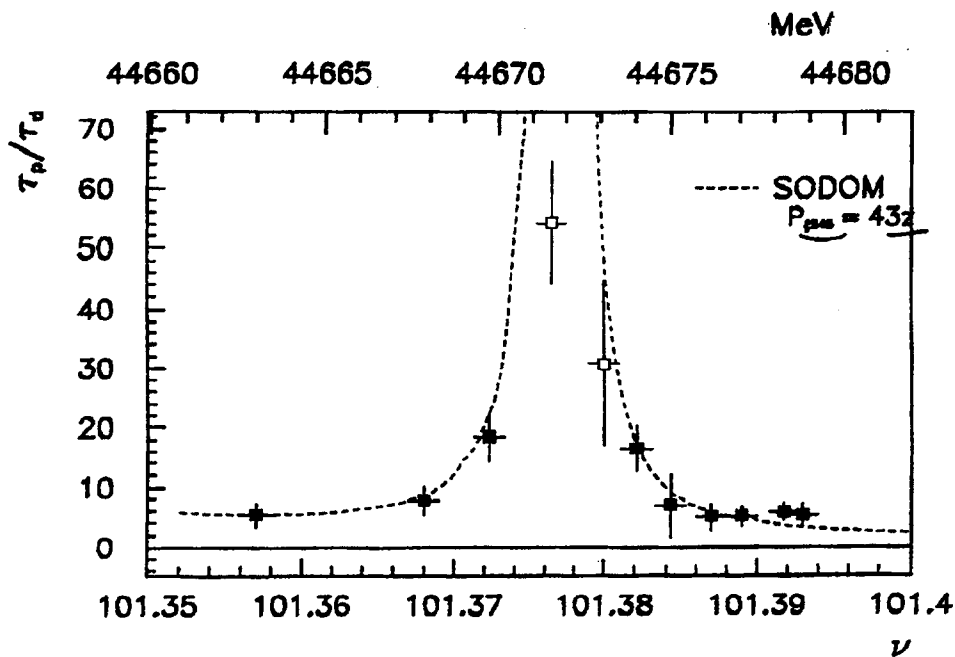


Fig.26: Measured and predicted synchrotron satellite in LEP [51]

- SITROS [62] is a Monte-Carlo tracking of the orbital and spin coordinates of a sample of particles. It was used to assess the possibility of observing polarization at the LEP energy and is presently used in HERA. The limitations of this approach are related to the requirements in computer time. To keep it reasonable, it is necessary to simplify grossly the quantum excitation by lumping the photon emissions in only a few azimuths. The number of tracked particles is necessarily limited. The core of the distribution is therefore well simulated but not the tails where strong depolarization is expected. Yet the rather good agreement between SITROS predictions and measured polarization at HERA seems to validate the model [19] (Fig. 27). At LEP, the disagreement between SITROS and SODOM results, the SITROS approach yielding more polarization, have not yet been resolved.

This rapid overview of the non-linear or higher-order phenomena shows that this field is still the subject of research and experimentation. Other approaches are now being developed, such as using Lie algebraic techniques to carry out perturbation expansions [69]. More

experiments at high energy are necessary to probe the theories. An accurate estimate of the threshold energy at which polarization would disappear is not yet possible.

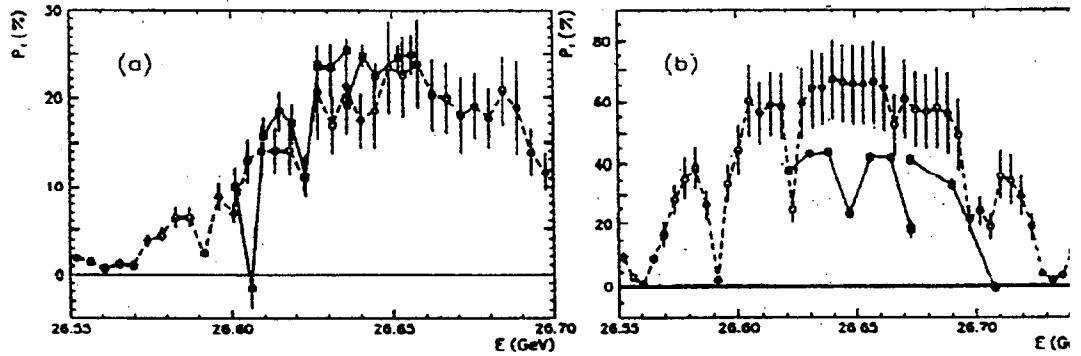


Fig. 27: Comparison between the measured polarization in HERA before and after optimization [19] and the SITROS predictions.

With the search and maximization of the polarization in HERA, Tristan and LEP, a wealth of new data is suddenly available. It is instructive to compare these data with the scaling law for the polarization *in the linear approximation*. According to formulae (65, 66), the asymptotic polarization should scale like:

$$P_{\infty} = \frac{8}{5\sqrt{3}} \frac{1}{1 + (\alpha E)^2} \tag{72}$$

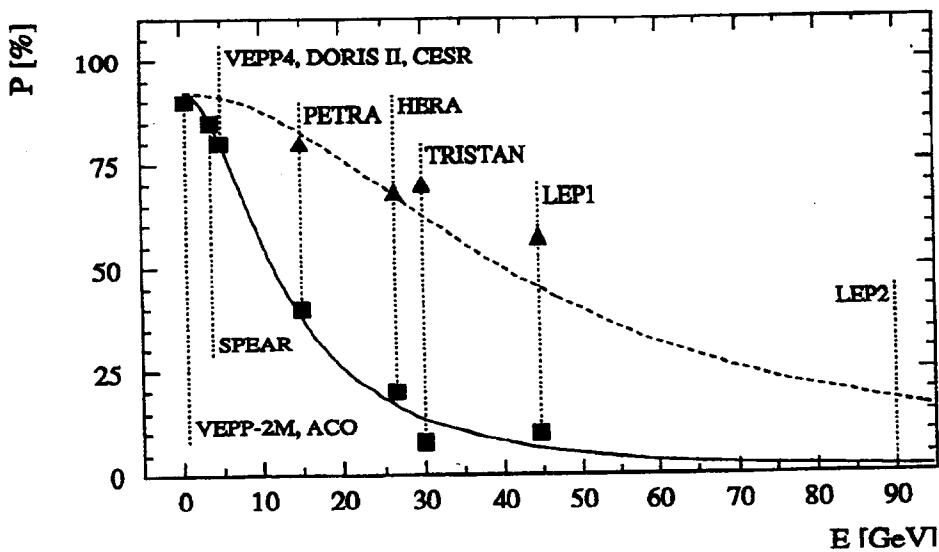


Fig. 28: Comparison between the predictions of the linear approximation and the measured polarization data, before and after harmonic spin matching.

It is remarkable that the measured data (figure 28) are almost perfectly compatible with the linear approximation. Yet the higher-order resonances are already observed at 3.7 GeV (Fig. 23) and above. This shows that the width of the higher-order spin resonances is still small compared to their spacing up to the highest energy reached so far, i.e. 46 GeV in LEP. If the working point is carefully chosen away from higher-order spin resonances, the asymptotic polarization is well predicted by the linear theory.

4.2.6 Depolarization by the beam-beam effect

In a beam-beam collision, the electro-magnetic field of one beam causes a precession of the spins of the particles in the second beam. Since SPEAR and VEPP-2M, collisions of polarized beams have not been required by physics and the expected depolarization not studied in depth. There was an experimental indication [43] at PETRA that at higher energy the beam-beam interaction can reduce the equilibrium polarization above the beam-beam limit. Nowadays, at energies comparable to the mass of the Z boson, where the electro-weak interactions dominate in the e^+e^- or ep collisions, there is a new interest for experiments with polarized beams. More information on the depolarization by the beam-beam effect is awaited before deciding on their feasibility.

4.3 Maximization of the polarization

4.3.1 Minimization of the depolarization

As can be seen from figure 28, the natural polarization decreases rapidly with increasing energy. For example, the expected polarization in LEP is less than 2% in standard physics conditions. It is possible to increase this expectation by minimizing the machine imperfections, optimizing their correction and by a careful choice of the machine parameters:

- In large machines, the alignment of the magnets is critical. The mere correction of the orbit with respect to beam monitors generally locally aligned on the near-by quadrupoles does not guarantee a good compensation of the spin rotations. Figure 29 shows the calculated polarization in LEP for given misalignments and residual orbits after correction. The results are averaged over a sample of random imperfections [70]. Realigning LEP vertically with the tightest tolerance has indeed provided the calculated increase in natural polarization.
- The most efficient correction of the vertical orbit is essential. The quality of the beam position monitors and their number set the limits of the correction capabilities. For example, in LEP, the 90° lattice was abandoned for a lattice with 90° in the horizontal plane but 60° in the vertical plane, thus increasing the sampling of the vertical orbit. This, together with improved beam monitors, allowed the rms residual orbit deviation to be decreased from a typical 1 mm to 0.3 mm. The correction of the orbit with a number of orbit correctors larger than strictly necessary reduces the vertical dispersion function significantly. This in turn reduces the excitation of the synchrotron spin resonance as may be inferred from (69).

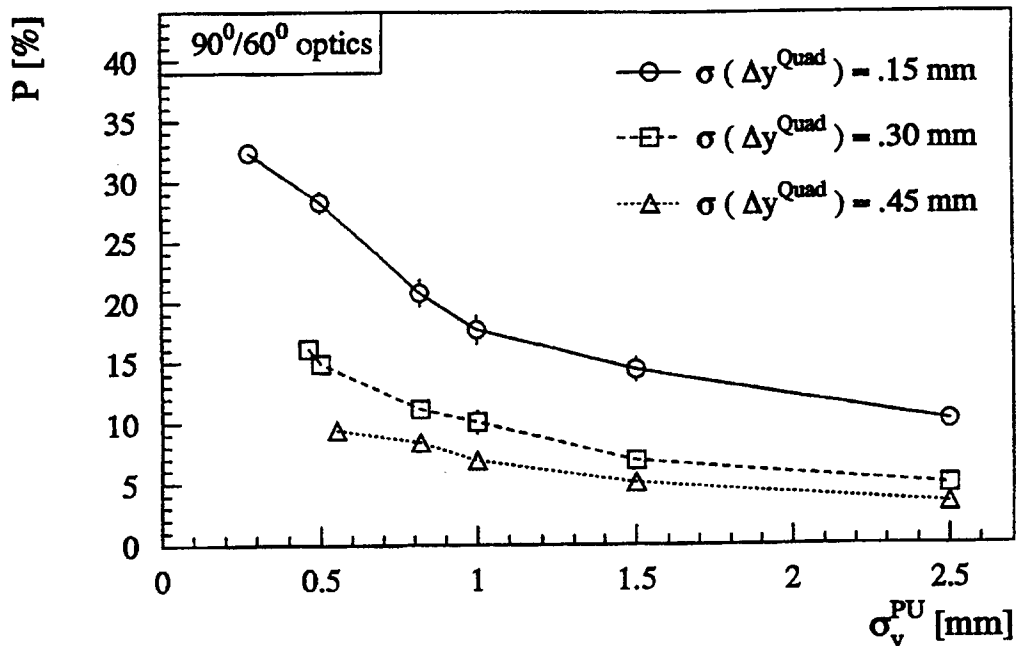


Fig.29: Dependence of the polarization on the machine alignment in LEP [70]

- A careful choice of the beam eigentunes $\{Q_x, Q_z, Q_s, \nu\}$ maximizes the ‘natural’ polarization level. The spin tune, i.e. the beam energy, should be selected with an integer part far from multiples of the ring superperiodicity (see section 2.4.4). The requirement of obtaining polarization at a given beam energy to calibrate a particle mass may lead to changing the integer parts of the betatron tunes, so as to avoid the strong integer systematic resonances (see section 2.4.3). At the LEP energy, these resonances do not allow polarization to develop; the physics optics was matched to obtain betatron tunes optimal for obtaining polarization at the Z mass. The fractional part of the spin tune should be close to $1/2$, yet away from higher-order satellites of linear resonances. Their density was minimized in LEP by choosing a synchrotron tune such that the upper and lower sidebands of the linear resonances are superimposed. The fractional parts of the betatron tunes should be as low as possible so that low-order satellites are as far as possible from the half integer.

4.3.2 Minimization of the tilt of the \mathbf{n} -axis

In the high-energy storage rings, the global minimization of the depolarization sources is not sufficient to reach a high polarization level. It becomes necessary to improve the equilibrium polarization by the so-called spin-matching procedure, which aims at making the ring more spin-transparent. The first step is to minimize the deviation of the spin closed solution \mathbf{n} from the vertical. We saw in section 2.4.3 that this deviation is large on integer spin resonances. It is furthermore possible to show that the depolarizing effect associated with the tilt of the \mathbf{n} -axis decreases with the 4th power of the distance between the spin tune and the integer spin resonance [e.g. 54]. One is thus naturally guided to a compensation of the two near-by integer spin resonances. The method is known as harmonic spin matching. Its principle is to generate

an horizontal field which is stationary in the $(\mathbf{l}, \mathbf{m}, \mathbf{n})$ spin frame and to adjust its amplitude and phase so as to compensate the driving term of each integer resonance. In other words, the perturbing horizontal magnetic field

$$\Delta B(s) = K(s) \cdot y_{co}(s) \quad (73)$$

due to the vertical displacement of the orbit $y_{co}(s)$ in the quadrupole gradient $K(s)$ is Fourier analysed. The angle in this analysis is the angle of the orbit in the laboratory frame α . The spin precession ψ is then

$$\psi = h\alpha \quad (74)$$

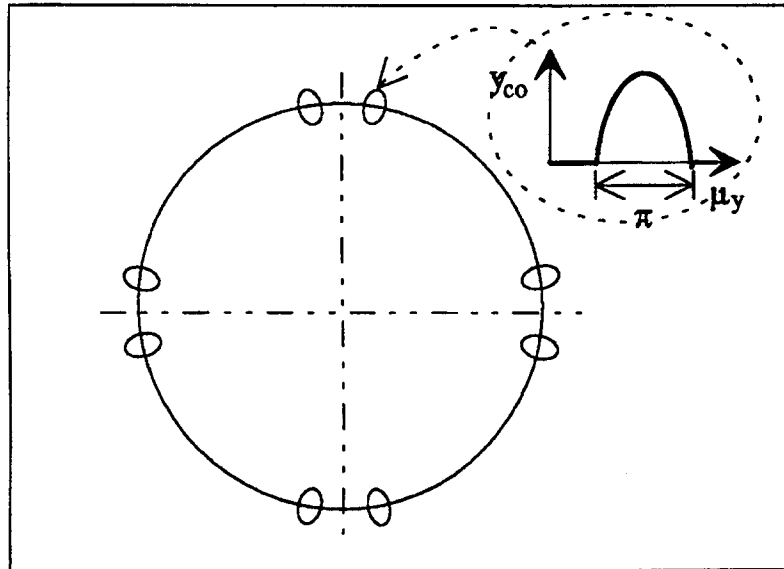


Fig.30: In HERA, LEP and Tristan, a pattern of vertical π -bumps in the arcs is used to produce the sine and cosine magnetic field harmonics necessary to compensate the near-by integer spin resonances

with the h harmonic number. The spin resonance compensation is achieved by generating opposite harmonics using a pattern of vertical orbit correctors. However the offending harmonics do not affect the closed orbit in a visible way (typically less than 0.1 mm) as they are far from the betatron tunes. Depending on the sensitivity of the beam position monitors, their compensation can be either empirical or computed from the measured orbit. The empirical procedure has been successfully applied at PETRA [49], where it allowed the polarization to be increased from 40% to 80%. The formalism was generalized to non-flat machines, e.g. including spin rotators[70]. Since then, the method was improved in LEP by observing that the

generation of horizontal field harmonics could be economically achieved by a few short vertical closed orbit bumps rather than by an orbit perturbation all around the ring (fig. 30).

Figure 31 shows the optimization in HERA where the sine and cosine components of the two near-by interger resonances are compensated. In LEP the very slow rise-time of the polarization would jeopardize an empirical compensation. This was a strong incentive to upgrade the beam monitoring system with the best technology. Figure 32 shows a harmonic analysis of the vertical closed orbit in the vicinity of the spin tune (103.47) before and after a calculated correction. Figure 33 shows the abrupt change of slope of the polarization build-up after the compensation was applied. The same technique was used at TRISTAN [50], where it allowed the polarization to be increased to 75%, and in proton rings (see section 3.2).

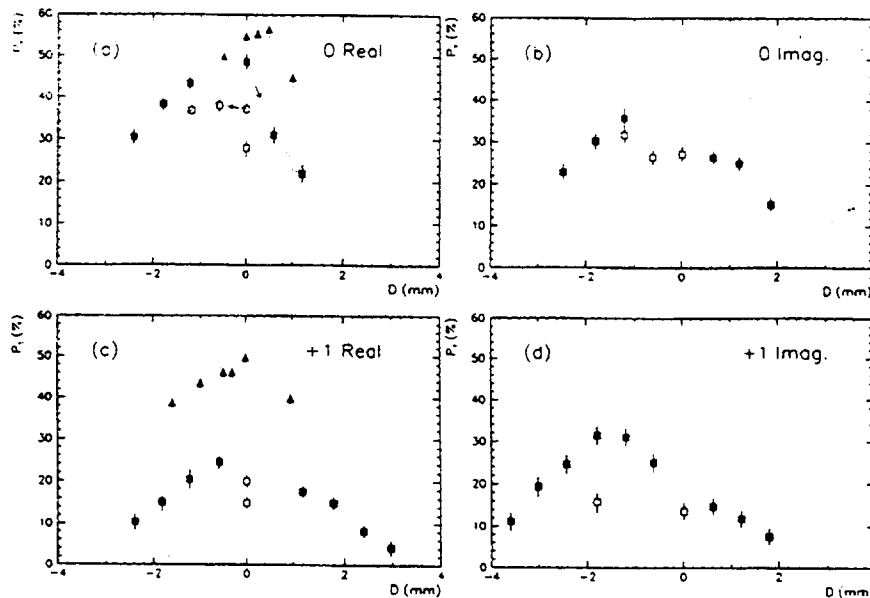


Fig.31: Optimization of the polarization at HERA by harmonic spin matching; the two parameters of the two closest integer resonances are compensated by trial and error. [19]

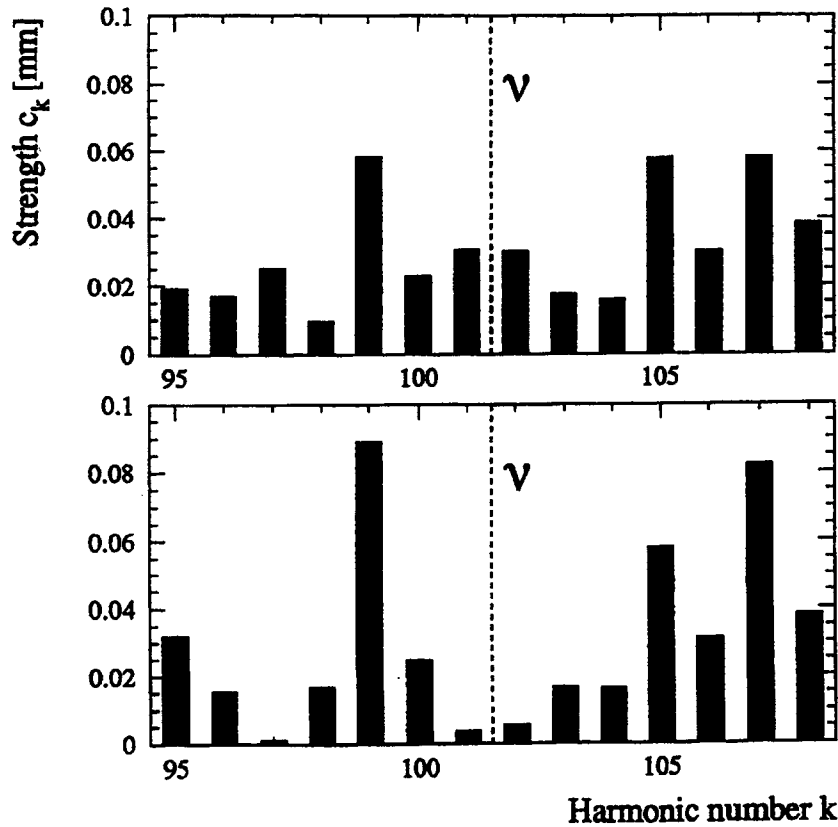


Fig.32: Harmonic analysis of the LEP vertical closed orbit in the spin precession frame. Figure a) shows the spectrum before harmonic correction, figure b) after correction. [51]

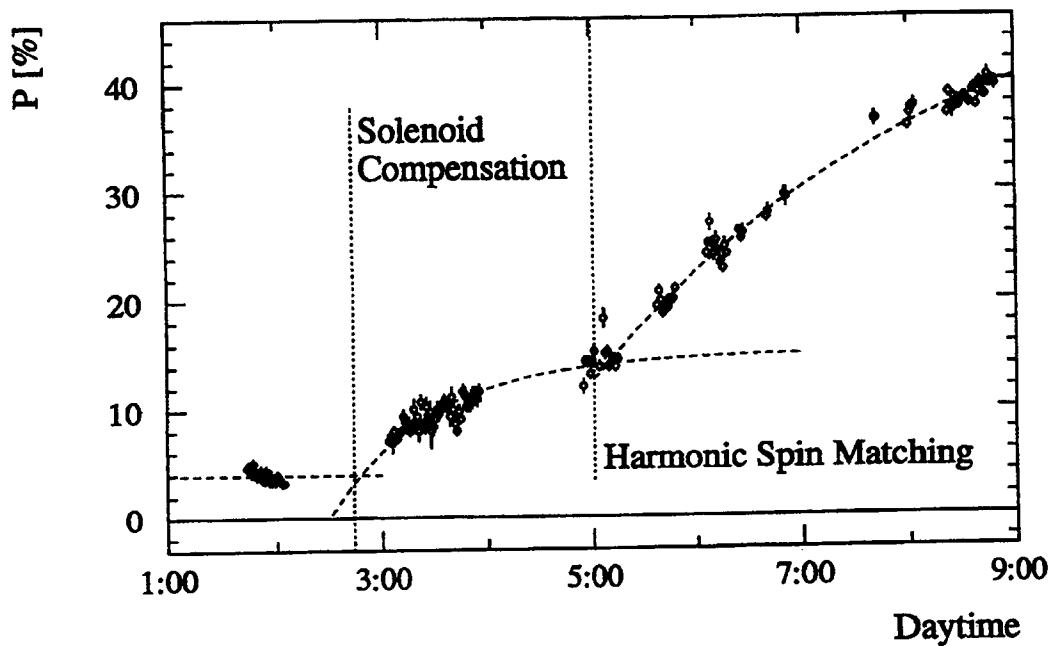


Fig. 33: Improvement of the polarization build-up in LEP following a calculated harmonic correction of the vertical orbit. [51]

4.3.3 Minimization of the Spin-orbit Coupling Vector \mathbf{d}

The high polarization levels recorded in Table 2 were all obtained by harmonic spin matching of the integer resonances. Yet, formulae (63, 64, 65, 66) shows that the depolarization is due to the betatron and synchrotron spin resonances and not to the integer resonances. As already introduced in section 2.4.3, the reason for the efficiency of the harmonic spin matching can be found by a close examination of the spin-orbit coupling integrals (67), (68), (69). In the general case of a moderate deviation of the \mathbf{n} axis from the vertical, they can be approximated as follows:

$$\mathbf{J}_s \approx \oint K e^{i\psi} (D_y - D_x |\delta \mathbf{n}| e^{i\psi_0}) ds \quad (75)$$

$$\mathbf{J}_x \approx \oint |\delta \mathbf{n}| e^{(i\psi + \psi_0)} (K \sqrt{\beta_x} e^{\pm i\phi_x}) ds \quad (76)$$

$$\mathbf{J}_y \approx \oint e^{i\psi} (K \sqrt{\beta_y} e^{\pm i\phi_y}) ds \quad (77)$$

At high energy, because of the large beam energy spread, the synchrotron spin resonances \mathbf{J}_s are overwhelming. The horizontal betatron resonances \mathbf{J}_y are also somewhat excited by betatron coupling while the vertical betatron resonances \mathbf{J}_x are rather weak. The two main depolarizing resonances are thus directly dependent on the tilt of the \mathbf{n} -axis. When the orbit is well corrected, this term is generally dominant in \mathbf{J}_s .

Although the polarization levels reached with harmonic spin matching are rather respectable, there is an incentive to compensate more exactly the spin-coupling integrals at high energy. It can indeed be shown that the strength of the higher-order spin resonances are proportional to the strength of the corresponding linear resonances. By compensating the former beyond the requirement for negligible linear depolarization, one can hope to weaken the higher-order depolarization and increase the threshold above which polarization disappears. Figure 34 shows the polarization calculated both linearly and by tracking with SITROS for LEP with very strong asymmetric wigglers, causing a beam energy spread at 45 GeV equivalent to the natural energy spread at 90 GeV. The four near-by integer spin resonances are corrected, assuming perfect beam position monitors. In which case, the spin-orbit coupling integral \mathbf{J}_s becomes the Fourier transform of the vertical dispersion function modulated by the quadrupole gradient, assuming an integer spin tune (formula (75)). This term was corrected for $\nu = 104$ by exciting compensating dispersion harmonics. In the vicinity of the integer, the polarization is calculated to reach then very high values. The difficulty of this compensation lies in the requirement of generating dispersion harmonics without orbit harmonics. Fortunately these harmonics are evaluated in the spin precession frame which does not rotate in the straight sections. Dispersion generated by orbit bumps in the straight sections meets the above-mentioned requirement.

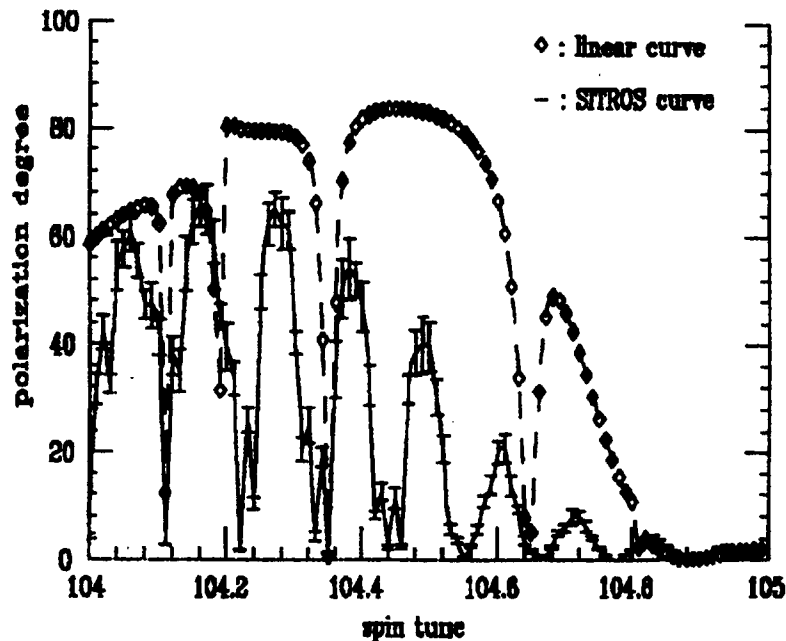


Fig. 34: Calculated polarization in LEP with strong asymmetric wigglers after complete compensation of the synchrotron spin-orbit coupling integral at $\nu = 104$.

It is equally possible to create harmonics of the focusing to compensate the depolarization by the betatron spin resonances. The interested reader is referred to Ref.[49].

4.4 Spin rotators

Spin rotators are special insertions which allow the \mathbf{n} vector to be rotated. They take advantage of the non-commutativity of finite rotations to break the proportionality relationship between the spin precession and the orbit rotation (Eq. (15)). Spin rotators may be used to restore the \mathbf{n} vector in its vertical position if it was tilted away by, e.g. experimental solenoids. A second aim is to decouple the spin tune and the energy, so as to allow easy acceleration without spin resonance crossing. These insertions, called Siberian snakes, were analysed in section 3.3. The main purpose of the 90° spin rotators is to rotate the polarization vector from its natural vertical position to the longitudinal position at the interaction point and back to the vertical position before entering the accelerator arc. Indeed, the experimental study of the electroweak interactions in e^+e^- annihilations or collisions calls for longitudinal helicity states.

4.4.1 Compensation of the solenoids

The field of the experimental solenoid is generally along the nominal orbit. It therefore does not disturb the closed orbit, but causes the spin to rotate about the horizontal direction. The skew quadrupoles generally used to cancel the betatron coupling do not restore the spin direction. The tilt of the \mathbf{n} vector propagates all around the machine and causes, in the case of LEP, an almost complete depolarization. Because it was necessary to obtain polarization in

physics conditions, small spin rotators were positioned on each side of each solenoid to restore the vertical position of the \mathbf{n} -axis in the arcs. This was in fact done merely by using four vertical closed orbit bumps positioned at the beginning of the arc [72]. Figure 35 shows the projection of the \mathbf{n} -axis onto the horizontal direction. The bump amplitudes (some 6 mm) were adjusted for an exact cancellation of the precession in the solenoid. The calculated polarization increased from 2% to more than 75%. Although the depolarization is here sufficiently and elegantly corrected, this example shows that restoring the \mathbf{n} -axis is very effective but not sufficient to achieve complete spin transparency.

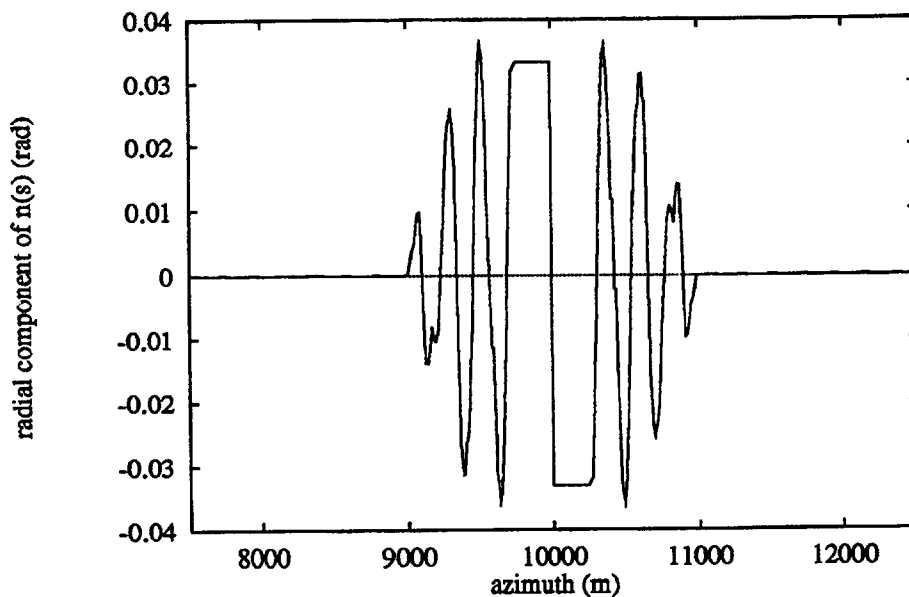


Fig.35: Two spin rotators per solenoid compensate the precession of the \mathbf{n} vector. The solenoid is positioned at the antisymmetry point.

4.4.2 Spin rotation at the interaction points

The requirement of a longitudinal spin is incompatible with the Sokolov-Ternov polarizing mechanism. For that reason, the polarization must remain vertical in the arcs, where most of the synchrotron radiation is emitted. In an interaction region, the spin closed solution \mathbf{n} is first bent into the beam direction by a first 90° spin rotator before the collision point. Then a second rotator bends it back to the vertical direction before entering the next arc. These two rotators are two sets of bending magnets with an antisymmetric configuration w.r.t. the collision point in the vertical plane. The antisymmetry has the advantage to leave the vertical closed orbit unperturbed in the arcs. There are many ways to bend the spin by a combination of horizontal, vertical and possibly longitudinal rotations. The choice of a solution involves an optimization process taking into account the depolarizing effect of the rotators, the allowable vertical emittance increase, the energy range where the spin is to be rotated, the synchrotron radiation background to the experiment, the possibility of tilting the detectors to match an inclined orbit.

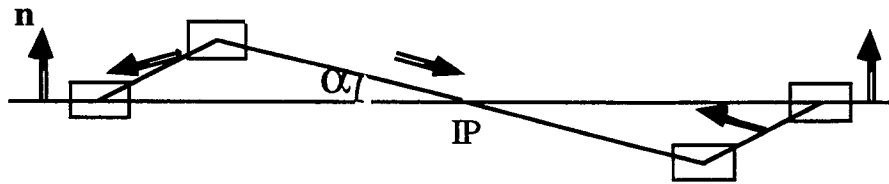


Fig. 36: Schematic side view of an S-bend configuration of two spin rotators antisymmetric w.r.t. the collision point IP. Each rotator consists of two magnets vertically bending the electron trajectory by an angle α and -2α respectively. With $\alpha = \pi/(2\gamma a)$ the spin closed solution \mathbf{n} is longitudinal at the IP.

The simplest configuration [73] of rotators is an S-bend, made of four vertically bending magnets (Fig. 36). It produces a vertical orbit displacement around the collision point, where the orbit crosses the median plane at a vertical angle α . Since the spin rotation angle is γa larger than the bending angle (15), the 90° rotation required to align the spin vector along the orbit results from the inclination of the latter by $\alpha = \pi/(2\gamma a)$. In the example of the S-bend rotators proposed [74] for LEP at 46 GeV, the vertical orbit slope is $\alpha = 15$ mrad, requiring a corresponding tilt of the physics detectors.

If for some reason the spin rotation is not exactly 90° , the spin is not exactly longitudinal at the interaction point: the asymmetry of the scheme guarantees however that the spin is rotated back to the vertical in all cases. This example illustrates a common difficulty of the spin rotators. Energy changes or the need to change the helicity state to avoid systematics requires the geometry of the accelerator to be changed locally. In HERA, where a large flexibility is required, a more involved rotator, the so-called mini-rotator [75], was designed. It is made of sandwiches of horizontally and vertically bending magnets arranged to match the separation of the electron and proton beams on both sides of the interaction point where they collide head-on on the nominal orbits. The displacement of the orbit in its tuning range from 27 GeV to 35 GeV was minimized to 20 cm by a proper sequence of horizontal and vertical rotations. The helicity can be reversed. This flexibility is made possible by installing the spin rotators on movable jacks.

Inside any of the possible rotators, the spin closed solution \mathbf{n} is bound not to be parallel to the magnetic field of the rotator dipoles. In the latter, the Sokolov-Ternov mechanism tends to polarize the beams along a field direction different from \mathbf{n} . The result is an ultimate polarization degree lower than the maximum 92.4%. The reduction is quantitatively given by the formula (55) in which the scalar product $\mathbf{b} \cdot \mathbf{n}$ becomes lower than one in the rotator magnets. The polarization decrease can only be minimized by an optimization of the rotator magnet configuration, in particular by using long magnets with low fields. Practical designs allow for polarization levels in excess of 80% at the highest energy. The real difficulty with spin rotators is that, unlike the case of the solenoid compensation, the \mathbf{n} vector is far from vertical in the spin rotator insertion. This causes the spin-orbit coupling vector \mathbf{d} not to vanish all along the ring circumference. At the energy of HERA, a single spin rotator reduces

significantly the polarization. At LEP it almost disappears. To overcome this effect, spin transparency must be restored.

4.4.3 Spin transparency conditions

The spin rotator can be considered as a very large defect which causes the spin-orbit coupling integrals $J_{\pm x, z, s}(s)$ to become large. The conditions for spin transparency are, on the contrary, that, whatever the azimuth s of a photon emission, the spin-coupling integrals integrated from s should vanish. This translates into ten conditions per magnet. Fortunately, unlike the ring imperfections, the defects introduced by the spin rotator are known. The same conditions are valid for most magnets and optics symmetries decrease further the number of constraints. Furthermore perfect spin transparency entails that all spin resonances are compensated. This would be a council of perfection, as we saw that the depolarization is mainly caused by a limited number of close-by spin resonances. In practice, it is possible to reduce the number of conditions to a manageable number [76]. The spin matching involves an adjustment of the quadrupole gradients to minimize the spin-orbit coupling integrals at least in some energy range, i.e. spin tune range. In LEP the spin transparency conditions were calculated analytically and converted into optics constraints handled by the matching module of the MAD program. Figure 37 shows the polarization calculated before and after spin matching of a possible LEP spin rotator [74].

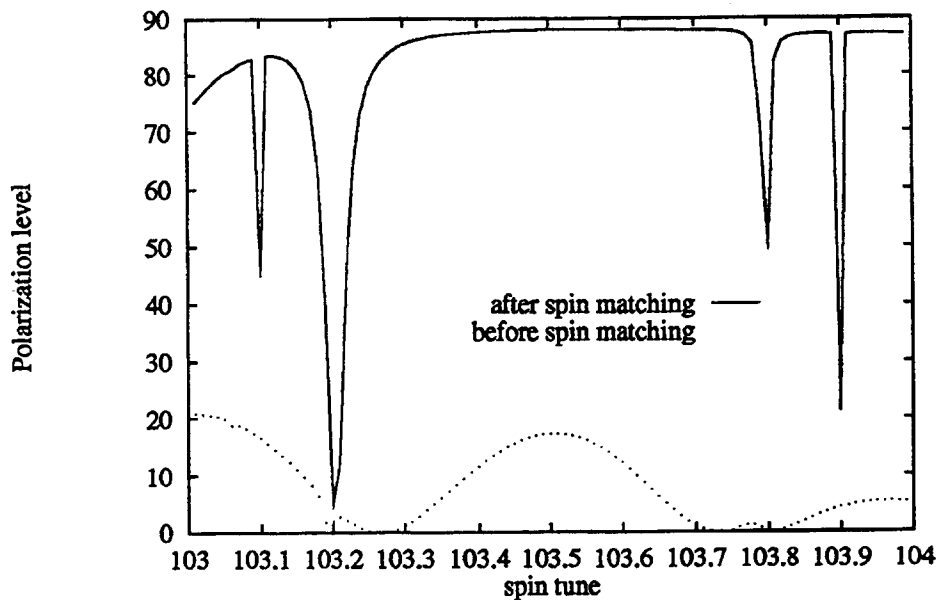


Fig.37: Calculated polarization in LEP equipped with a spin rotator before and after spin matching [74]

For HERA, the dependence of the spin coordinates on the orbital coordinates was computed in the linear approximation. The requirement was then to adjust the focusing so as to minimize the submatrix expressing the spin-orbit coupling. Figure 38 shows the calculated polarization in HERA with the spin-matched rotator [77]. In spring 1994, the HERA spin

rotator was installed and tested. Its spin matching was sufficiently effective to avoid any loss of polarization at a level of 70% [78].

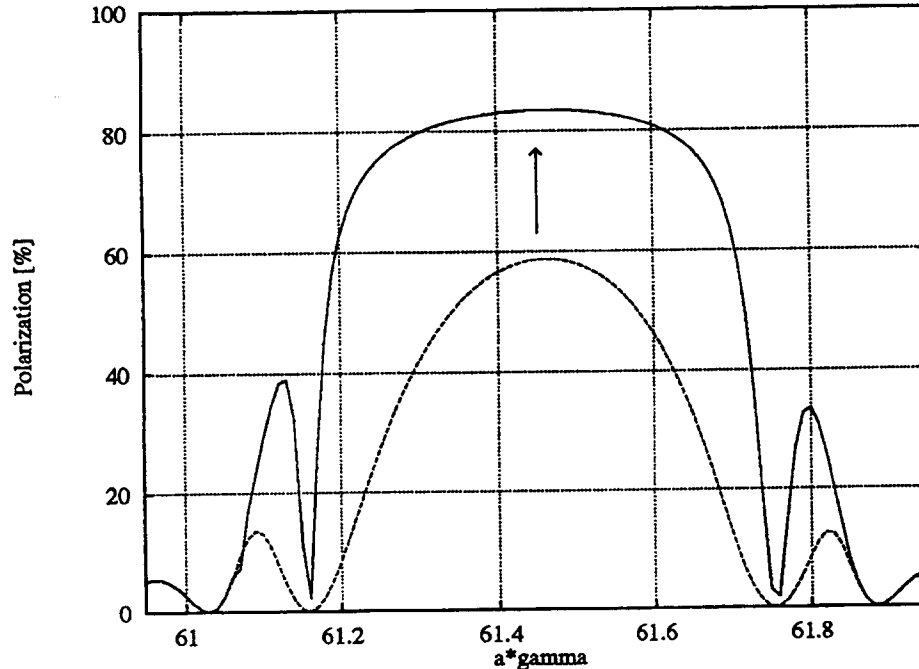


Fig.38: Calculated polarization in HERA equipped with a spin rotator before and after spin matching [77].

4.5 Energy calibration by depolarization on an artificial RF spin resonance

The first application of transverse beam polarization in an electron storage ring is the accurate calibration of the beam energy. This has been carried out in several rings : VEPP2-M [79], BESSY [44], VEPP4 [80], DORIS II [81], CESR [48] and LEP [82]. The method used is based on a RF resonance technique. It can be done even with a modest degree of polarization. The principle is similar to a NMR experiment, although the magnetic energy absorbed by the beam is too small to be directly measured as in NMR experiments.

At LEP the RF resonance technique has been applied to measure the Z mass and width at 44.7, 45.6 and 46.5 GeV corresponding to a spin tunes of 101.5, 103.5 and 105.5. As soon as the polarization reaches about 10%, a small radial RF magnetic field, produced by a kicker, is turned on. The applied field excites a RF spin resonance. The tune value of that resonance is varied by slowly changing the frequency of the RF field. When the scanned range of tune overlaps the spin tune of the beam, the RF resonance is crossed, and the beam is depolarized (Fig. 39). To determine the RF frequency at which depolarization occurs the central frequency is varied and the polarization is continuously monitored with the polarimeter. From that measurement the spin tune and the energy of the beam are deduced. In contrast to a proton beam accelerated in a synchrotron, the spin tune of the beam is fixed and the tune of the RF spin resonance is varied.

The RF magnetic field has a very small integral value, about 4 Gm only. For the spin motion this radial field is a perturbing field which can be analyzed in frequency to find the spin

resonances that it excites, as explained in Section 2.4. The tunes of these RF resonances are given by :

$$\nu = n \pm \frac{f_{RF}}{f_{rev}} \quad (78)$$

where f_{RF}, f_{rev} are the applied RF and revolution frequencies respectively and n is any integer. The frequency span is typically 112 Hz per minute corresponding to a spin tune range of 0.002 and an energy range of 0.9 MeV. The beam energy E is deduced from the frequency f_{RF} at which depolarization is observed :

$$E = \frac{m_0 c^2}{a} \left(n \pm \frac{f_{RF}}{f_{rev}} \right) \quad (79)$$

after lifting the sign ambiguity (obtained by observing the change of the depolarization frequency when the energy is varied). The limit in accuracy of this calibration method can be as small as 10^{-5} . It is limited by the imperfections of the real storage rings: if the spin rotations are not all about the vertical axis, the spin precession per turn is not anymore strictly proportional to the energy and formula (78) is not exact [83]. The perturbation is less than 0.5 MeV at LEP for a polarization level of 10%. Other limitations are related to non-linearities (sextupoles), interference with other spin resonances,....

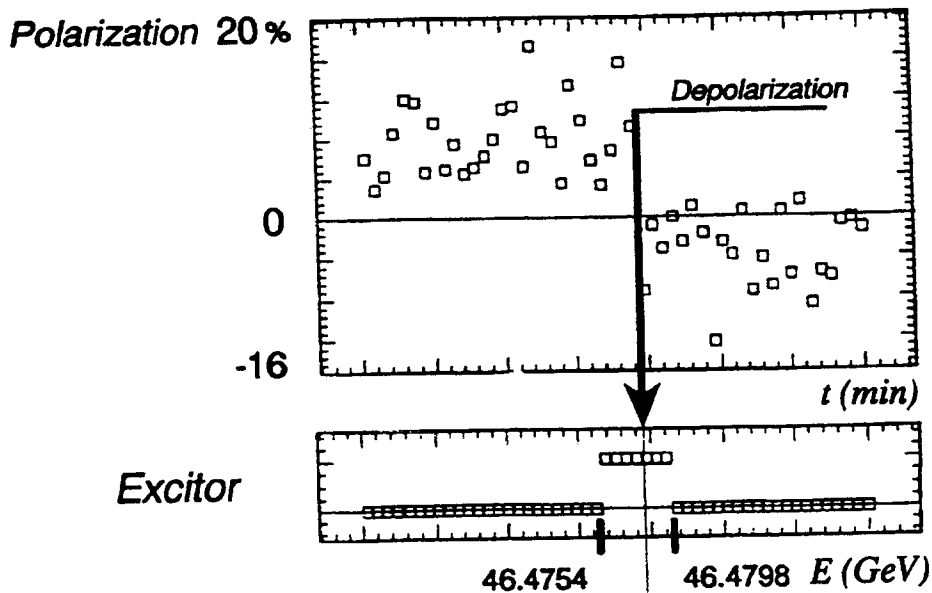


Fig. 39: The polarization versus the time in a calibration experiment at LEP. Depolarization is observed when the RF field (excitor) is turned on with a frequency span corresponding to an energy range (4.4 MeV) overlapping the beam energy E .

The energy calibration by resonant depolarization has also been used to measure the mass of the K mesons [84,85], ϕ meson [86], ψ meson [87] and of the $\Upsilon, \Upsilon', \Upsilon''$, mesons [46,48,79,88,89]. One must also mention the very accurate comparison [90] of the gyromagnetic anomaly of electrons and positrons at VEPP2-M by again a RF technique similar to an NMR experiment showing that the sophisticated spin manipulations in Nuclear Magnetic Resonance can also be used in electron storage rings.

ACKNOWLEDGEMENTS

The authors wish to thank the colleagues of the different laboratories who provided the referenced data and figures. J. P. K. thanks R. Assman, A. Blondel, D. Barber, A. Hofmann and the LEP Polarization Collaboration for many discussions and comments.

BIBLIOGRAPHY

- [I] J.S. Bell, Introduction to the concept of polarization in particle beam, Report CERN 75-11 (1975).
- [II] A. Chao, Calculation of the electron polarization in the linear approximation (SLIM), Fermilab Summer School 1981, AIP Conf. Proc. n° 87, p. 395
- [III] E.D. Courant and R. Ruth, Acceleration of polarized protons, Report BNL-51270 (1980)
R. Ruth, Proc of the 12th Int. Conf. on High-Energy Accelerators (Fermilab, 1983) p. 286.
- [IV] B.W. Montague, General review on polarization in high-energy rings, Physics Reports, Vol. 113 (1984).
- [V] A.A. Sokolov and I.M. Ternov, Synchrotron radiation and spontaneous polarization, 'Radiation from Relativistic Electrons', AIP Translation Series, New-York (1986).

REFERENCES

- [1] R. F. Schwitters et al, Phys. Rev. Lett., 35 (1975), 1320.
- [2] F. Lehar, Colloq.Phys. (France) n0 C-6 (1990), 19.
- [3] A.N. Skrinskii and Yu. M. Shatunov, Sov. Phys. Usp. 32(6) (1989) p. 548.
- [4] M. Froissart and R. Stora, Nucl. Instr. Meth., 7 (1960) 297.
- [5] V. Bargmann, L.Michel, V.L.Telegdi, Phys. Rev. Lett. 2 (1959) 435.
- [6] I.M.-Ternov, Yu. M. Loskutov, L.I. Korovina, Sov. Phys. JETP, 14 (1962), 921.
- [7] A. A. Sokolov and I. M.Ternov, Sov. Phys.-Doklady, 8 (1964) 1203.

- [8] R. Belbéoch et al, in Proc. USSR Nat. Conf. Particle Accelerators (1968) p. 129.
- [9] The Orsay Storage Ring Group, in Proc. 8th Int. High Energy Accelerators CERN, Geneva, 1971) p. 127.
- [10] V. N. Baier, Sov. Phys.-USPEKHI, 14 (1976) 1063.
- [11] S. I. Serebnyakov, Sov. Phys.-JETP, 44 (1972) 695.
- [12] T. Khoe et al, Part. Accel., 6 (1975) 213.
- [13] T. Aniel et al., Colloq.Phys. (France) N0 C-2 (1985), 499.
- [14] P. A. Chamouard et al., Colloq. Phys. (France) n0 C-6 (1990), 569.
- [15] F. Z. Khiari et al., Phys. Rev. D, 39 (1989) 45.
- [16] W. Brefeld et al, Nucl. Instr. Meth., 228 (1985) 228.
- [17] C. Y. Prescott et al., Phys. Lett., 77B (1978) 347.
- [18] C. Y. Prescott, SLAC-PUB-6242 and Proc. 2nd Intl. W. on Physics and Exp.at Linear Colliders, Waikoloa, Hawai (1993)
- [19] D.P. Barber et al. Nucl. Instr. Meth. A338 (1994), 166.
- [20] K.Nakajima et al, Proc. 3rd EPAC, vol.1 (1992), 919.
- [21] L. Knudsen et al, Phys. Lett., 270B (1991) 97.
- [22] E. D. Courant and R. D. Ruth, BNL Report, 51270 (1980).
- [23] R. D. Ruth, IEEE Trans. Nucl. Science, 30 (1983) 286.
- [24] Tkatchenko, 1990 EPAC Conf., ed. P. Marin and P. Mandrillon (Nice,1990) p. 159.
- [25] A. W. Chao, AIP Conf. Proc., 87 (1981) 395.
- [26] A. W. Chao, IEEE Trans. Nucl. Science, 30 (1983) 2383.
- [27] D. P. Barber, 1990 EPAC Conf., Ed. P. Marin and P. Mandrillon (Nice,1990) p. 164.
- [28] Particle Data Group, J. J. Hernandez et al., Phys. Lett. B, 239 (1990).
- [29] CODATA Recommended values, Journ. of Research of NBS, 92 (1987) 85.
- [30] J. S. Bell, Report, CERN 75-11 (1975).
- [31] L. T. Thomas, Phil. Mag. 3 (1927) 1.
- [32] J. D. Jackson, Classical Electrodynamics (J. Wiley and sons, 2nd ed.,1975) p.541.
- [33] Ya. S. Derbenev and A. M. Kondratenko, Sov. Phys.-Dokl., 20 (1976) 562.
- [34] Ya. S. Derbenev et al, Part. Acc., 8 (1978) 115.
- [35] K. Steffen, DESY HERA report, 82/02 (1982).
- [36] J.P.Koutchouk, Proc. 8th Symp.High Energy Spin Phys. vol. 2 (1988), 1004.
- [37] N. Horikawa, in Proc. 9th Int. Symp. on High Energy Spin Physics, ed. K.-H. Althoff and W. Meyer (Springer-Verlag, 1991) p. 172.
- [38] A. D. Krisch, Phys. Rev. Lett., 63 (1989) 1137.
- [39] J. E. Goodwin, Phys. Rev. Lett., 64 (1990) 2779.
- [40] P. A. Chamouard, private communication.
- [41] Ya. S. Derbenev and A. M. Kondratenko, Novosibirsk preprint, 78-74 (1978).

- [42] J. D. Jackson, *Rev. Mod. Phys.*, 48 (1976) 417.
- [43] J. S. Bell and J. M. Leinaas, *Nucl. Phys. B*, 284 (1987) 488.
- [44] K. Ott, private communication and BESSY Annual Report 1988.
- [45] J. R. Johnson et al, *Nucl. Instr. Meth.*, 204 (1983) 261.
- [46] A. S. Artamonov et al, *Phys. Lett.*, 118B (1982) 225.
- [47] D. P. Barber, DESY report, M-83-29 (1983).
- [48] W. Mackay et al, *Phys. Rev.*, 29 (1984) 2483.
- [49] H. D. Bremer et al, DESY report, 82-026 (1982).
- [50] K. Nakajima et al, Paper TUS04A at the 1992 EPAC Conf. (Berlin 1992).
- [51] R. Assmann et al., CERN Report, CERN SL 94-08 (AP), (1994).
- [52] V.N. Baier et al., *Sov. Phys. JETP*, 31 (1970), 908.
- [53] J. Buon, LAL/RT/83-01 (1983).
- [54] B. W. Montague, *Physics Reports*, 113 (1984)
- [55] M. Sands, SLAC-121, (1970), 118.
- [56] Ya. S. Derbenev and A. M. Kondratenko, *Sov. Phys.-JETP*, 37 (1973) 968.
- [57] L. N. Hand and A. Skuja, *Phys. Rev. Lett.*, 59 (1987) 1910.
- [58] D. P. Barber and S. R. Mane, *Phys. Rev. A*, 37 (1988) 456.
- [59] J. Buon, LAL/RT report, 84-05 (1984).
- [60] A. Chao, K. Yokoya, DESY M-82/09, (1982), K9, R19.
- [61] A. W. Chao, *Nucl. Instr. Meth.*, 180 (1981) 29.
- [62] J. Kewisch et al., *Phys. Rev. Lett.* 62, (1989), 419.
- [63] H. Grote, CERN Report, SL-DI 91-20, (1991).
- [64] Ya. Derbenev et al., *Part.Accel.* 9, (1972), 247.
- [65] J. Buon, *Part. Acc.*, 32 (1990) 153.
- [66] S. R. Mane, Fermilab report, FN-466 (1987).
- [67] K. Yokoya, KEK Report 92-6, (1992).
- [68] H. Grote, CERN Report SL/92-56 (AP), (1992).
- [69] Yu. Eidelmann, V. Yakimenko, Proc. 1991 IEEE Part. Conf. , San Francisco, (1991), 269.
- [70] R. Assman, Proc. 3rd Work. on LEP Perf., CERN SL/93-19 p.341 (1993)
- [71] D.P. Barber et al., DESY 85-044, (1985).
- [72] A. Blondel, LEP Note 629, (1990).\$
- [73] V. N. Baier, *Sov. Phys.-USPEKHI*, 14 (1972) 695.
- [74] H. Grote et al, 1990 EPAC Conf., Ed. P. Marin and P. Mandrillon (Nice,1990),1 497.
- [75] J. Buon and K. Steffen, *Nucl. Instr. Meth.*, A 245 (1986) 248.
- [76] J. Buon, *Nucl. Instr. Meth.*, A 275 (1989), 226.
- [77] D. Barber, M. Boege, E. Gianfelice, private communication.

- [78] D. Barber et al., to be published.
- [79] Ya. S. Derbenev et al, Part. Acc., 10 (1980) 177.
- [80] A. E. Bondar et al, in Proc. 12th Int. Conf. on High Energy Accelerators, ed. T. Cole and R. Donaldson (Fermilab 1983) p. 240.
- [81] D. P. Barber et al, Phys. Lett., 135B (1984) 498.
- [82] L. Arnaudon et al, CERN Report, SL/92-16 (1992), to be published in Phys. Lett. B, (1992).
- [83] R. Assmann, J.P. Koutchouk, CERN SL/()ç-13 (AP) (1994).
- [84] L. M. Barkov et al, Nucl. Phys., B148 (1979) 53.
- [85] L. M. Barkov et al, Novosibirsk preprint, 83-85 (1983).
- [86] A. D. Bukin et al, Yad. Fiz., 27 (1978) 976.
- [87] A. A. Zholents et al, Phys. Lett., 96B (1980) 214.
- [88] A. S. Artamonov et al, Phys. Lett., 137B (1984) 272.
- [89] S. E. Baru et al, Z. Phys. C, 30 (1986), 551.
- [90] I. B. Vasserman et al, Phys. Lett., 198 (1987), 302.